AMERICAN UNIVERSITY OF BEIRUT

HYDRODYNAMIC CHARACTERIZATION OF TUBULAR REACTORS/CONTACTORS EQUIPPED WITH SCREEN-TYPE STATIC MIXERS

by
KHALED MOHAMAD J. ABOU HWEIJ

A thesis
submitted in partial fulfillment of the requirements
for the degree of Master of Engineering
to the Department of Mechanical Engineering
of the Faculty of Engineering and Architecture
at the American University of Beirut

Beirut, Lebanon
April 2015

AMERICAN UNIVERSITY OF BEIRUT

HYDRODYNAMIC CHARACTERIZATION OF TUBULAR REACTORS/CONTACTORS EQUIPPED WITH SCREEN-TYPE STATIC MIXERS

by

KHALED MOHAMAD J. ABOU HWEIJ

Approved by:

Prof. Fouad Azizi, Assistant Professor — Advisor
Department of Mechanical Engineering/ Chemical Engineering Program

Prof. Kamel Abou Ghali, Professor — Member of Committee
Department of Mechanical Engineering

Prof. Mahmoud Al-Hindi, Assistant Professor — Member of Committee
Department of Mechanical Engineering/ Chemical Engineering Program

Date of thesis/dissertation defense: April 27, 2015

AMERICAN UNIVERSITY OF BEIRUT

THESIS, DISSERTATION, PROJECT RELEASE FORM

Student Name: Abou Hweij Khaled Mohamad J.

Last First Middle

⊗ Master's Thesis ○ Master's Project ○ Doctoral Dissertation

☒ I authorize the American University of Beirut to: (a) reproduce hard or electronic copies of my thesis, dissertation, or project; (b) include such copies in the archives and digital repositories of the University; and (c) make freely available such copies to third parties for research or educational purposes.

☐ I authorize the American University of Beirut, **three years after the date of submitting my thesis, dissertation, or project,** to: (a) reproduce hard or electronic copies of it; (b) include such copies in the archives and digital repositories of the University; and (c) make freely available such copies to third parties for research or educational purposes.

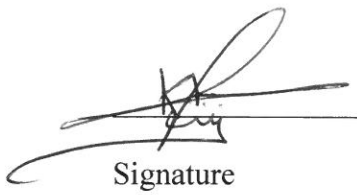

Signature

30-April-2015

Date

ACKNOWLEDGMENTS

I would like to extend my gratitude to the people who contributed to bring this research project to fruition. First and foremost, I thank my advisor, Professor Fouad Azizi, for accepting me in his group. I am so deeply grateful for his help, professionalism, valuable guidance and financial support through this project and through my entire program of study that I do not have enough words to express my sincere appreciation.

My sincere thanks also go to my committee members who never spared an effort to help and provide their valuable feedback. Special thanks to Prof. Kamel Abou Ghali and Prof. Mahmoud Al-Hindi for their guidance and for accepting to be on my thesis committee board.

I would like to acknowledge my family who supported me during my graduate studies. I would like to thank Mom, Dad, and Walid. Moreover, I could not have survived the road without the love of an awesome group of friends who knew enough not to stray too far when I needed some time alone. I would like to send my special thanks to Mohamad Merhi, Mohamad Baassiri, Hussein Maaneih, and Samer Doudar. I owe a debt of gratitude to all my friends, those I had the chance to meet in this graduate school and they were good enough not to throw me overboard while at sea.

AN ABSTRACT OF THE THESIS OF

Khaled Mohamad J. Abou Hweij for Master of Engineering
Major: Mechanical Engineering

Title: Hydrodynamic Characterization of Tubular Reactors/Contactors Equipped with Screen-Type Static Mixers

This work discusses the characteristics of a single phase liquid and two-phase gas-liquid flow through tubular reactors/contactors equipped with screen-type static mixers from a hydrodynamic and macromixing perspective. The effect of changing the screen geometry, number of mixing elements, reactor configuration, and the operating conditions, were investigated by using four different screen types of varying mesh numbers.

For this reason, in the single phase flow study, pressure drop was measured over a wide range of flow rates ($2{,}300 \leq Re \leq 21{,}500$) and was found to increase with a decreasing mesh opening. Friction factor values are also reported in the work, but when compared to other types of motionless mixers, screen-type mixers were found to require much lower energy requirements with very low recorded Z values ($1.15 \leq Z \leq 5$) that are two to three orders of magnitude lower than those reported for other motionless mixers. While in two-phase gas-liquid flow study, pressure drop was measured over a wide range of flow rates ($11{,}500 \leq Re \leq 28{,}000$) and was found to increase with a decreasing mesh opening. However, the efficient dispersion of the gas phase in the presence of screens and the consequent generation of microbubbles, was found to reduce the drag coefficient of the screen and hence reduce the pressure drop with an increase in the gas holdup.

Furthermore, in the single phase liquid phase study, residence time distribution experiments were conducted in the transitional and turbulent regimes ($2{,}300 \leq Re \leq 11{,}500$), where they were conducted in the turbulent regime ($18{,}900 \leq Re \leq 29{,}200$) in the gas-liquid flow study. Using a deconvolution technique the RTD function was extracted in order to quantify the axial/longitudinal dispersion.

In both single phase liquid and two-phase gas-liquid flow studies, the findings highlight that regardless of the number and geometry of the mixer, reactor configuration, and/or operating conditions, axial dispersion coefficients that are lower than those of an empty pipe were always recorded. Further, the wire diameter and mesh opening were found to directly affect the axial dispersion in the reactor. However, it was found that axial dispersion increases with a larger number of mixing elements in the two-phase gas-liquid flow, but has a smaller effect in the single phase liquid flow.

NOMENCLATURE

Symbol	Description	Unit
b	Screen wire diameter	(m)
$C(t)$	Normalized concentration of tracer	(–)
$C_{in}(t)$	Concentration of tracer measured at the inlet	(mol/L)
$C_{out}(t)$	Concentration of tracer measured at the inlet	(mol/L)
$C(\omega)$	FFT of the sampled inlet concentration	(–)
COV	Coefficient of variation	(–)
D	Empty pipe diameter	(m)
D_{ax}	Axial dispersion coefficient	(cm^2/s)
$E(t)$	Residence time distribution function	(–)
f	Fanning friction factor	(–)
f_i	Fanning friction factor calculated based on the screen open area	(–)
k	Total number of sampled points	(–)
L	Length of the mixing zone	(m)
L_M	Total distance of the mixing section	(m)
L_p	Distance between pressure transducers	(m)
M	Screen mesh opening	(m)
Mn	Mesh number	
MSE	Mean squared error	(–)
N	Number of screen elements in the system	(–)
Ne	Newton number	(–)
p	Fitting exponent	(–)
Pe	Péclet number	(–)
Q	Volumetric flow rate	(L/min)
Re	Empty pipe Reynolds number	(–)
Re_b	Wire Reynolds number	(–)
Re_{jet}	Macroscopic jet Reynolds number	(–)
Re_M	Mesh Reynolds number	(–)
$S(\omega)$	FFT of the smoothing formula	(–)
t	Time	(s)
t_m	Mean residence time calculated from RTD	(s)
U	Superficial flow velocity	(m/s)
U_G	Gas-phase velocity	(m/s)
U_L	Liquid-phase velocity	(m/s)
U_{mix}	Mixture velocity	(m/s)
V	Volume of the mixing zone	(L)
z	Axial position in the pipe	(m)

Greek Symbols

α	Fraction open area of the screen	(–)
γ	Fitting parameter	(–)
ΔP	Pressure drop in the mixing zone	(kPa)
Θ	Dimensionless time	(–)
μ	Viscosity	(kg/m·s)

ρ	Density	(kg/m^3)
σ^2	Variance	(s^2)
τ	Theoretical residence time in the mixing zone	(s)
ϕ	Dispersed phase volume fraction	(–)
Ψ	Drag coefficient	(–)

CONTENTS

ILLUSTRATIONS

Figure

TABLES

Table

GENERAL INTRODUCTION

Static mixers are defined as motionless elements introduced into a continuous fluid flow path in reactors/contactors. Static mixers were not widely employed in process industries before 1970s. Nowadays, they are considered as major replacements for conventional agitators as they are capable of achieving better performance (Al Taweel et al., 2013; Ghanem et al., 2014). The absence of any mechanical part in these static mixers naturally reveals lower energy consumptions and reduced maintenance. They require small space with less equipment costs and no required power except the pumping energy for flowing fluid. However, providing a minimum residence time, static mixers deliver homogenized feed streams, as they can be manufactured to meet different standards for most materials. Motionless mixers can serve in single pass reactor, recycle loop reactor, mechanically agitated tank in recycle loop, conventional batch and in continuous stirred tank reactor with unmixed feed streams (Thakur, 2003).

Static mixers are designed as identical elements that are easily inserted in pipes or reactors/contactors. They disturb the fluid particles and redistribute them in the radial and tangential directions, thus creating turbulence and homogenizing the fluid without intending to change the pipe diameter and flow rate. As turbulent regime is achieved, eddy diffusion promotes adequate mixing in the fluid flow, yet changing the velocity profiles (Ghanem et al., 2014; Lobry et al., 2011; Thakur et al., 2003). Moreover, motionless mixers attain better dispersion properties in both single and multiphase flow in reactors/contactors. They contribute to better mass and heat transfer rates with more energy efficient manners, hence achieving better mixing conditions (Al Taweel et al., 2013; Ghanem et al., 2014; Madhuranthakam et al., 2009; Peschel et al., 2012; Thakur et al., 2003). Static mixers are optimized by some adjustable parameters according to

their applications, where the number of elements and aspect ratio are regularly adjusted (Thakur, 2003).

Static mixers are involved in essential mixing processes in industries. Motionless mixers promote mixing of miscible fluids as well as immiscible organic phase. However, heat transfer enhancement and dispersion of gas into liquid in continuous liquid phase is well achieved in miscible fluids. Static mixers effectiveness evident in mixing of mixable fluids is due to rapid diffusion and conduction processes. They are also commonly used in liquid-liquid systems, gas-liquid systems, solid-liquid systems and solid-solid systems. Commercial static mixers are used into many applications. Low viscosity mixing and mass transfer in gas-liquid system (Koch-Glitsch Inc.), dilution of feed to reactor, blend out thermal gradient in viscous stream (Rose Engineering Inc.) blending catalyst, dye or additive into viscous fluid (Rose Engineering Inc.) are among industrial applications. Static mixers are frequently used in food processing, petrochemical and refining, pharmaceutical and cosmetics, paints and resins, water and waste water treatment industries (Thakur, 2003).

Static mixers act differently according to their different configurations. They are classified into five different families. Open designs with helices (Kenics (Chemineer Inc.)…), open designs with blades (Low pressure Drop (Ross Engineering, Inc.)), corrugated-plates (SMV (Koch-Glitsch, Inc.)), multi-layers designs (SMX (Koch-Glitsch, Inc.)) and closed designs with channels or holes (international surface generator- ISG (Ross Engineering INC.)) (Thakur, 2003).

Moreover, static mixer configurations are divided into four different groups according to their applications. They vary from mixing of miscible fluids to interface generation between immiscible fluids in addition to axial mixing and heat transfer operation and thermal homogenization. The first group describes the homogeneous

reactions, where highly chemical exothermic reactions are categorized under the heat transfer operation sets (Thakur, 2003).

Motionless mixers in axial mixing set are exclusively of new types with precise designs that endorse mixing to attain the residence time behavior as that in agitated or continuous stirred tank reactors/contactors (Thakur, 2003). However, this thesis is formatted as two separate manuscripts dealing with hydrodynamic and macromixing perspective in both single and two phase flow in tubular reactors equipped with screen-type static mixers. As the first chapter investigates single phase liquid flow whereas two-phase gas-liquid flow is discussed in chapter two. Each manuscript is an independent entity, having its own body sections.

CHAPTER I

Hydrodynamics and Residence Time Distribution of Liquid Flow in Tubular Reactors Equipped with Screen-type Static Mixers

A. Introduction

Multiphase flow phenomena play an important role in the chemical and process industries. Such processes include unit operations carried out in batch and continuous stirred tanks, bubble and liquid-liquid extraction columns, as well as airlift reactors, amongst others. Optimizing the performance, economy and safety of these multiphase reactors/contactors is therefore of paramount importance. A proper understanding of the mixing process, if attainable, combined with an ability to predict the dynamic properties of the dispersion, such as drop/bubble size distributions and mass transfer performance, would therefore allow the introduction and implementation of major enhancements. However, due to the complex hydrodynamic conditions prevalent in most commercially available contactors/reactors, such achievements remain unreachable. Consequently, designing these units remains heavily dependent on the employment of empirical knowledge, experience, and extensive pilot-scale testing.

Nonetheless, plug flow reactors/contactors serve as a better choice when compared to other multiphase contactors/reactors in order to understand the complex phenomena taking place as well as providing better performance and control over mixing, breaking of drops and bubbles, as well as temperature. The growing interest in the use of tubular reactors equipped with static mixers, over conventional mixers, emanates from their inherent advantages whereby better performance can be achieved at lower capital and operating costs. Findings in the literature highlight the higher multiphase mass transfer and reaction rates that could be achieved in energy efficient manners while simultaneously handling large flow rates and achieving high heat removal or addition rates (AL Taweel et al., 2013; Ghanem et al., 2014; Thakur et al., 2003). Furthermore, the insertion of properly-selected static mixing elements into tubular reactors allows for the introduction of the various reactants at different points

along the reactor length, thereby facilitating the achievement of optimal temperature and reactant concentration profiles that are required to achieve optimal selectivity and conversion.

Woven mesh screen-type static mixers have been used to repetitively superimpose an adjustable, radially-uniform, highly-turbulent field on the nearly plug flow conditions encountered in high velocity pipe flows (Azizi and Al Taweel, 2011). The very high energy dissipation rates present in the thin region adjacent to the screen are particularly effective in processing multiphase systems. This not only helps in the formation of fine dispersed phase entities (bubbles and/or drops) but also considerably enhances the value of the interphase mass transfer coefficient (Al Taweel et al., 2005, 2007, 2013; Azizi and Al Taweel, 2011). This is evidenced by their ability to promote contact between different phases, where interfacial areas as high as 2,200 m2/m3 (Chen, 1996), and volumetric mass transfer coefficients, k_La, as high as 4.1 s-1 (Azizi, 2009) could be achieved in the case of gas-liquid systems. In processing liquid-liquid systems, k_La values as high as 13 s-1 (Al Taweel et al., 2007) were attained which enabled for 99% of equilibrium conditions be achieved in less than 1 s. This can be mainly attributed to the impact that high-intensity microscale turbulence, typically encountered in this mixer configuration, can have on the dispersed phase mass transfer coefficient (Azizi and Al Taweel, 2012). In other terms, such good performance, which is attributed to not only the formation of very fine dispersed phase entities but also enhanced mass transfer coefficients, is credited to the very high grid-generated turbulence and the consequent elevated micro-mixing intensities generated in the regions adjacent to the screens (Bourne and Lips, 1991).

Similarly to other static mixers, screen-type mixers also offer the flexibility of designing the reactor to meet various mixing and/or energy requirements. For example,

whereas a short inter-screen spacing favours the production of fine dispersions that are typical of high mass transfer rates and fast reactions, a longer spacing would be favourable for conditions of slow reactions and/or low energy requirements. However, changing the reactor configuration and/or the operating conditions will impact the performance of the reactor by affecting its mixing efficiency and consequently the characteristics of the flowing dispersion along its length.

A frequently used technique to understand and quantify the actual flow phenomena in reactors/contactors is the residence time theory. This concept has been in place for over a hundred years (Nauman, 2008) and became widely used after the work of Danckwerts in the early 1950's (Dankwerts, 1953; Nauman, 2008). Residence time distribution (RTD) is an indicator of the macro-mixing in the reactor as it measures features of ideal or non-ideal flows associated with bulk flow patterns, and knowledge concerning its characteristics would therefore offer the ability to adapt the reactor/contactor design to meet specific process requirements.

RTD in static mixers, e.g. SMX, Kenics, etc…, was studied experimentally by several investigators for both Newtonian and non-Newtonian fluids (Harris et al., 1996; Häfeli et al., 2013; Kemblowski and Pustelnik, 1988; Keshav et al., 2008; Madhuranthakam et al., 2009; Nauman, 1982; Nauman et al., 2002; Pustelnik, 2986; Rafiee et al., 2013; Wadley and Dewson, 2005; Ziolkowski and Marawski, 1987) . The majority of these studies focused on measurements in the laminar flow regime and reported the data in the form of the RTD function or one of its moments.

Consequently, this investigation deals with characterizing the macro-mixing in tubular reactors/contactors equipped with screen-type static mixers. This will be achieved by measuring the residence time distribution (RTD) function in the reactor under various operating conditions and geometrical/design configurations in order to

quantify the axial dispersion coefficient. In addition, the effect of varying the various operational parameters on the pressure drop of the reactor/contactor will also be reported and discussed.

B. Materials and Methods

The residence time distribution is determined experimentally by injecting an inert chemical, molecule, or atom into the reactor and measuring its concentration in the effluent stream as a function of time using a suitable measurement tool. For this purpose, dyes, salts, and radioactive elements amongst others, have commonly been used to measure residence time in a variety of reactors/contactors by means of measuring light intensity, conductivity and radioactivity, respectively. In addition, there exist several techniques of injection that can be used to measure the RTD, namely, pulse, step, and imperfect pulse, each of which has its advantages, disadvantages and a different method of analysis to extract the desired information from measurements. In the current study, a pulse injection of a highly concentrated aqueous salt solution was used to measure the RTD in the reactor/contactor by means of measuring the changes in electrical conductivity in reverse osmosis (RO) water of low initial conductivity. However, to mitigate the problems that might arise from entrance effects to the mixing section and the assumption of a perfect pulse input, the analysis was performed assuming an imperfect pulse technique. This was accomplished by measuring the electrical conductivity at both entrance and exit to the mixing section. The following section therefore describes the experimental setup used in this study in addition to the various experimental techniques employed for measuring RTD. Moreover, the method of analysis will also be detailed.

1. Experimental Setup

The continuous flow experimental set up used in the present investigation is schematically illustrated in Figure 1. Reverse osmosis (RO) water was collected in a 200 L tank from which it was fed to the static mixer loop using a constant speed

centrifugal pump (Pedrollo, model PKm80) . The manually regulated flow rate of water entering the mixing section was measured by means of a digital flow meter (Omega model: FP7002A) and was varied between 4 and 20 L/min for the RTD experiments (which corresponds to pipe Reynolds numbers ranging from ~2,300 to ~11,500). The reactor section consists of a 855 mm vertical transparent Plexiglas pipe (50.1 mm OD and 44.1 mm ID) in which the mixing section is 600 mm long. The reactor section was flanged to the setup and placed 700 mm downstream from the liquid entrance to ensure radial flow uniformity.

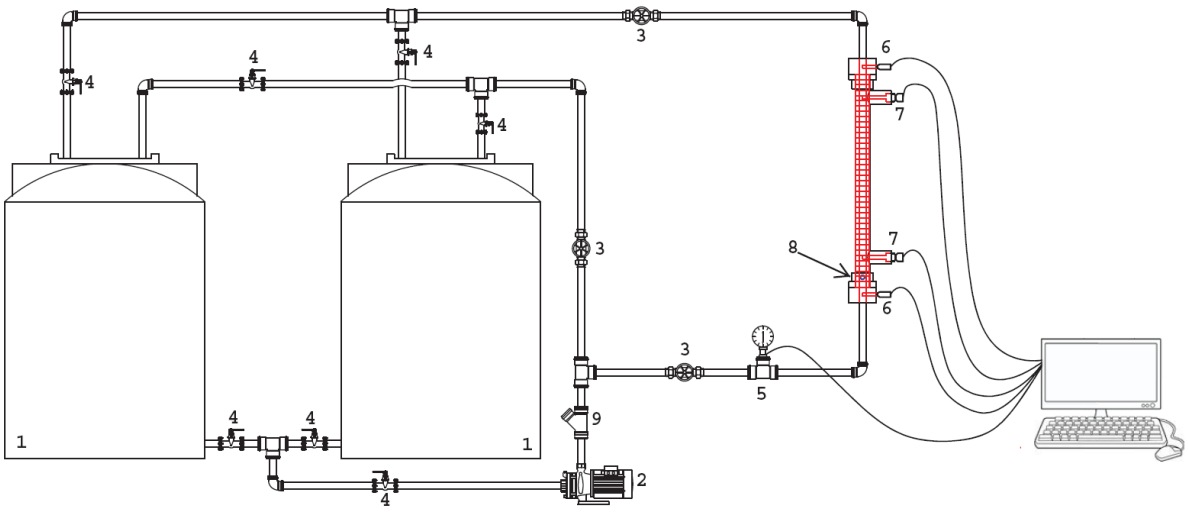

Figure 1: Schematic representation of the experimental setup (1) Supply/Drain tank, (2) centrifugal pump, (3) gate valve, (4) ball valve, (5) flow meter, (6) pressure sensors, (7) conductivity sensors, (8) injection port, (9) check valve.

Screen-type static mixing elements (the characteristics of which are given in Table 1 and their geometry represented in Figure 2) were held apart using a set of transparent Plexiglas cylindrical spacers (44 mm OD and 37 mm ID) placed inside the outer pipe. (Figure 3). Forty (40) spacers of 20 mm length were used and ensured that the screens remained perpendicular across the flow direction and helped maintain the inter-screen spacing at the desired value. The effective diameter of the mixing section

which contained a varying number of static elements is thus 37 mm with a total length of 600 mm.

Mesh Number	$M \times 10^3$ (m)	$b \times 10^3$ (m)	$(M - b) \times 10^3$ (m)	α (%)
20	1.27	0.4064	0.8636	46.2
30	0.8382	0.3048	0.5334	40.8
50	0.508	0.2286	0.2794	30.3
80	0.3175	0.1397	0.1778	31.4

Table 1 Characteristics of the investigated stainless steel plain-weave wire cloth

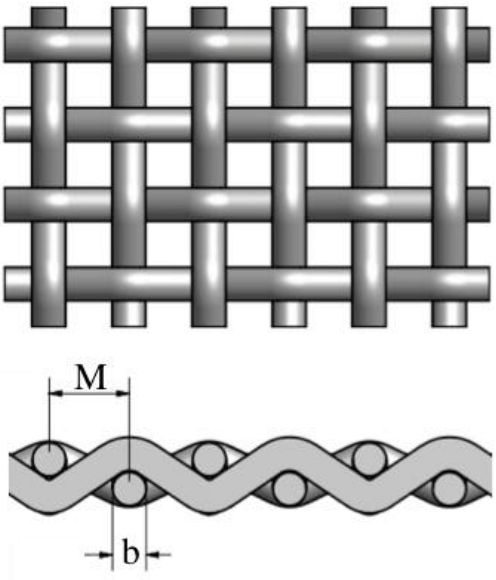

Figure 2: Geometry of the woven screen

The setup was provided with an injection valve through which the tracer pulse was injected, and two pressure transducers (Omega model PX302-015G) that were fixed at the top and bottom of the reactor section, 855 mm apart. Furthermore, conductivity measurements were taken at the inlet and outlet to the mixing section by means of two identical conductivity sensors (Omega model CDCE 90-X) placed at 75 and 675 mm from the injection point, respectively. The measurement cells of these conductivity sensors were aligned with the centerline of the pipe. Data from all sensors

was collected at a frequency of 10 Hz by means of a National Instruments data acquisition board (NI USB-6218) and a specially developed LabView program.

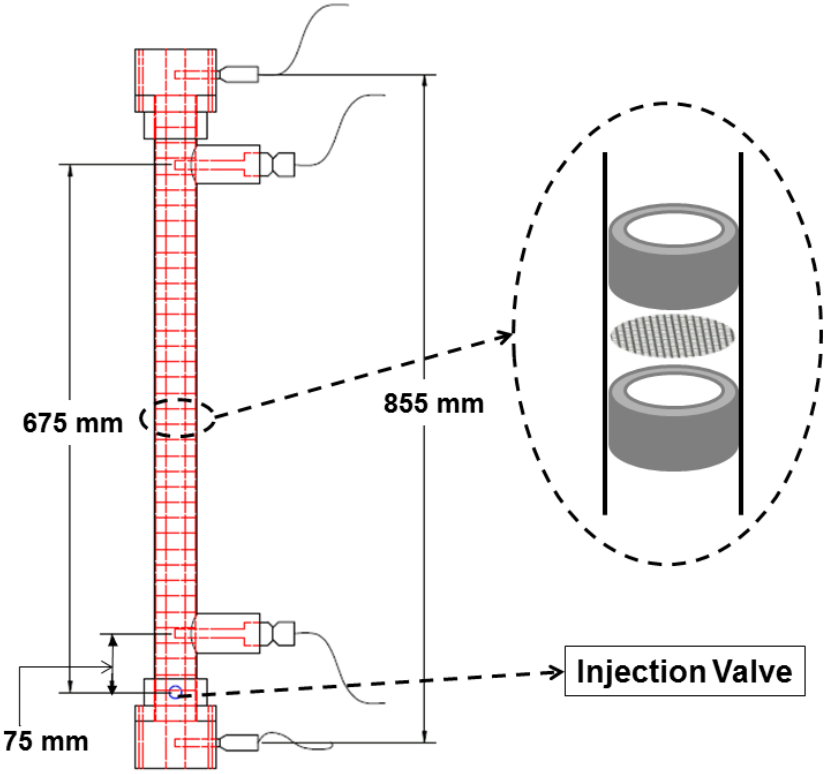

Figure 3: Internal configuration of the reactor section

In addition to studying the effect of varying screen geometries (as highlighted in Table 1) on the RTD, experiments were also conducted while varying the number of screen elements. Measurements were acquired in the presence of 1, 2, 4, and 8 screens inside the mixing section. Consequently, and based on the number of screens in the system, N_s, the inter-screen spacing, L, was changed to ensure a proper distribution of the screens over the entire mixing section volume while keeping this distance independent of the screen geometry. Whereas an inter-screen spacing of 300 mm was used in the presence of two screens, the distance was reduced to 120 mm for 4 screens and further decreased to 60 mm in the presence of 8 screens. Moreover, the first screen element was always held at 60 mm from the inlet conductivity sensor. The various flow

rates and the corresponding flow velocity and Reynolds number at which the RTD experiments were performed are detailed in Table 2.

It should be noted, that in the case of pressure drop experiments, data was collected with 8 screen-type static mixing elements in the system and the flow rate in the reactor unit was varied over a larger span ranging from 4 to 40 L/min, which corresponds to Re values between ~2,300 and 23,000. Such discrepancy between the flow rates depending on the type of experiment (RTD vs. pressure drop) was dictated by the inability of the conductivity sensors to detect the variation in the conductivity due to a pulse injection at higher velocities.

Q **(L/min)**	***U*** **(m/s)**	***Re*** **(–)**
4	0.062	2,300
6	0.093	3,450
8	0.124	4,600
10	0.155	5,750
12	0.186	6,900
15	0.232	8,600
20	0.310	11,500

Table 2 Operating conditions for RTD experiments

2. Experimental Method

To measure the residence time distribution inside the reactor/contactor, electrical conductivity was measured at both the inlet and outlet of the mixing section after imposing a pulse injection of a highly conductive solution in the low conductivity RO water (~ 200 μS) used in all experiments. To ensure that no accumulation of salt occurs, which would subsequently impose an increase in the initial conductivity of the water, RO water was drawn from one clean supply tank and the outlet of the mixing section was directly drained or collected in a separate tank.

Because of the linear relationship between its concentration and its electrical conductivity, an aqueous solution of potassium chloride, KCl, was used as the tracer in all experiments. A stock solution of 100 g/L corresponding to 1.34 mol/L was prepared using deionized water, from which 5.8 mL were repetitively injected in the system as a pulse disturbance. This volume was kept constant throughout the experiments by using the same injection syringe, and all injections were performed in less than 300 ms. Depending on the operating conditions, this meant the maximum conductivity would range between 2,000 and 3,000 μS, which is substantially larger from the base conductivity of the water.

3. Methodology

Ziolkowski and Morawski, (1987) studied the RTD in various types of motionless mixers including wire gauze or screen-type static mixers. Their study however only considered low Reynolds numbers ($200 < Re < 5{,}000$) as well as two different geometries of screen mixers, a small and a very wide mesh opening ($(M–b)$ = 0.5 and 3 mm, b = 0.3 and 1 mm, respectively). In addition, they fitted their measured concentration profiles using the well-known single-parameter axial dispersion model without attempting to find the RTD function, and concluded that this can only be employed over a very short range of Re and therefore proposed a two-parameter model to fit the concentration profiles instead. Their proposed model accounted for the velocity profile in the stream cross-section as well as a modified axial dispersion coefficient.

In the current work, however, the effect of varying the number of screens (1, 2, 4, and 8 screens) and screen geometry (four different geometries related together by a geometric progression, mesh size varying by a factor of ~1.6) in addition to operating at a larger Re range ($2{,}300 \leq Re \leq 11{,}500$) are investigated. Furthermore, in lieu of fitting

the concentration profiles with the single parameter model, this model will be employed to fit the RTD function that is obtained by analysing the inlet and outlet concentration profiles which are assumed to be imperfect pulses, and therefore a better accounting for the flow non-idealities. Such approach offers a better alternative to the assumption of a perfect Dirac delta pulse injection and/or not accounting for the RTD function in the analysis.

4. RTD analysis

Residence time theory is a well-established, mature technology that deals with measuring the time fluid particles spend inside the reactor vessel boundaries. Except for the special case of piston flow, velocity profiles and molecular diffusion will cause a distribution of residence times (Nauman, 2008). Typically, measuring the residence time distribution from a pulse injection, requires the monitoring of the outlet concentration of the tracer in order to obtain the exit-age distribution function, $E(t)$, which is defined in Equation (1).

$$E(t) = \frac{C(t)}{\int_0^\infty C(t)\,dt} \tag{1}$$

In other terms, $E(t)$ is a quantitative measure of how much time, different fluid elements spend in the reactor. Therefore mass continuity dictates that the E-function should obey the following constraint depicted in Equation (2).

$$\int_0^\infty E(t)dt = 1 \tag{2}$$

Furthermore, it is common to compare and analyze RTDs by means of their moments instead of their entire distributions, and typically the first two moments of the distribution are used. The first moment is the mean residence time and can be used as an indicator on whether there exist dead volumes or channeling in the reactor. This is

obtained by comparing the first moment of the distribution, t_m, defined in Equation (3), with the theoretical residence time, τ, that is calculated as the ratio of the reactor volume to the volumetric flow rate $\left(\tau = V/Q\right)$.

$$t_m = \int_0^\infty tE(t)dt \tag{3}$$

The second moment of the distribution is another important parameter that indicates the "spread" of the distribution and is calculated using Equation (4).

$$\sigma^2 = \int_0^\infty (t - t_m)^2 E(t)\, dt = \int_0^\infty t^2 E(t)\, dt - t_m^2 \tag{4}$$

Another important parameter is the coefficient of variation (COV) which reflects a combination of the first and second moments of the distribution (Harris et al., 1996; Thakur et al., 2003). The coefficient of variation, defined in Equation (5), is the ratio of the standard deviation to the mean and provides a measure of the relative spread of a distribution.

$$COV = \frac{\sigma}{t_m} \tag{5}$$

A complete distributive mixing is indicated by a value of $COV = 0$, while a $COV = 1$ is a sign of total segregation (Thakur et al., 2003).

Even though care was always taken while performing the pulse experiments, in order to eliminate all sources of error associated with the assumption of a perfect pulse, or flow disturbances while entering the reactor/mixing section, it was decided to use the imperfect pulse technique to analyze the residence time distribution. In this approach, the injected pulse is not a perfect Dirac distribution rather it has a certain spread. Therefore, by measuring the inlet and outlet conductivities, and consequently the inlet and outlet concentrations of the tracer, the residence time distribution function can be

obtained by the deconvolution of the inlet and outlet concentrations which are related by the convolution integral shown in Equation (6).

$$C_{out}(t) = \int_0^t C_{in}(t') \cdot E(t - t')\, dt' \tag{6}$$

5. Deconvolution Method

Several authors studied the numerical solution of the deconvolution integral (Bennia and Nahman, 1990; Boskovic and Loebbecke, 2008; Essadki et al., 2011; Guiterrez et al., 2010; Heibel et al., 2005; Hutter et al., 2011; Häfeli et al., 2013; Mills and Dudukovic, 1989; Moa et al. 1998; Nahman and Guillaume, 1981; Parruck and Riad, 1984; Pasnanakis and Abel, 1998; Saber et al., 2012; Thakur et al., 2003) and several techniques are available in the open literature for solving Equation (6) and extracting the impulse response or residence time distribution function, $E(t)$.

Most of these techniques call for solving the integral by using Fourier transforms after normalizing the concentration data, because convolution in the time domain corresponds to multiplication in the frequency or Laplace domain (Boskovic and Loebbecke, 2008; Mao et al., 1998). Typically, fast Fourier transforms can be used in lieu of discrete Fourier transforms. Therefore, by switching from time- to frequency-domain, the convolution integral using normalized concentrations becomes,

$$FFT\left(C_{out}(t)\right) = FFT\left(C_{in}(t)\right) \times FFT\left(E(t)\right) \Leftrightarrow C_{out}(\omega) = C_{in}(\omega) \times E(\omega) \tag{7}$$

and $E(t)$ can be obtained by calculating the inverse transform (*IFFT*) of the ratio of the Fourier transforms of the normalized outlet and inlet concentrations, as shown in Equation (8).

$$E(t) = IFFT\left(\frac{FFT\left(C_{out}(t)\right)}{FFT\left(C_{in}(t)\right)}\right) = IFFT\left(\frac{C_{out}(\omega)}{C_{in}(\omega)}\right) \tag{8}$$

Due to measurement noise, many high order harmonics will be created and consequently unrealistic oscillations of high frequency, and negative numerical values at many instants, will appear in the calculated $E(t)$. The former case being unlikely and the latter of no physical meaning (Mao et al., 1998).

To mitigate these problems, several investigators have therefore implemented noise filtering techniques (Bennia and Nahman, 1990; Hunt, 1971; Mills and Duduković, 1989; Nahman and Guillaume, 1981; Parrauk and Riad, 1984). In the current work, the filtering method presented by Mills and Duduković (1989), which relies on the method of regularization that was refined by Hunt (1970), Hunt (1971), and Mao et al. (1998) will be employed.

For details concerning the mathematical derivation, the reader is referred to the works of Hunt, (1970, 1971) and Mills and Duduković (1989). In this approach a second-order smoothing filter was employed to remove noise from measured data according to Equation (9).

$$E(\omega) = \frac{C_{out}(\omega)/C_{in}(\omega)}{1+\gamma \dfrac{S(\omega)\cdot S^{*}(\omega)}{C_{in}(\omega)\cdot C_{in}^{*}(\omega)}} \tag{9}$$

where, γ is the filtering parameter, and the term $\left[\gamma \cdot S(\omega)\cdot S^{*}(\omega)/C_{in}(\omega)\cdot C_{in}^{*}(\omega)\right]$ plays the role of a digital filter. $S(\omega)$ is the FFT of the smoothing formula coefficient series [1, –2, 1, 0, …, 0]; which is a matrix of length k, the number of sampling points. The quantities marked with an asterisk denote the complex conjugate (Hunt, 1970,1971; Mills and Duduković, 1989; Mao et al., 1998) . The length of the matrix, k, is equivalent to the number of sampled points in each experimental run.

While the filtering parameter is unbounded and can assume any positive value ($\gamma \in \mathbb{R}^{+}$), the choice of γ should be only remove the frequency components of the

errors and prevent over-smoothing by deleting essential frequency components of the solution (Mao et al., 1998). The authors Mao et al. (1998) proposed using the additivity property for the moments of the normalized tracer impulse responses (Levenspiel, 1972), in order to identify γ. This method relies on calculating the nth absolute moment using two methods. The first calculates it as the difference between the nth moment for the sampling and injection responses, whereas the second computes the nth moment directly from the estimated impulse response distribution. The appropriate value of the filtering parameter, γ, is therefore the one that minimizes the error between the two to below a prescribed error. However, this requires a preliminary estimate of γ, which can be obtained by solving a non-linear equation that relates the mean squared error (MSE) between the approximate and exact solutions for the impulse response as given by Hunt, (1971) and shown in Equation (10).

$$\mathrm{MSE} \cong k \cdot \sum_{i=0}^{k-1} \frac{C_{out}(i) \times C^{*}_{out}(i)}{\left[1 + \gamma^{-1} \dfrac{C_{in}(i) \times C^{*}_{in}(i)}{S(i) \cdot S^{*}(i)}\right]^{2}} \tag{10}$$

If an estimate of the MSE can be made, then a 1-D root finding method will permit a preliminary estimate of the filtering parameter γ.

In the current work, MatLab was used to perform these calculations after implementing a user defined function that would solve the equations to first obtain the value of the fitting parameter, γ, and consequently the impulse response, $E(t)$. Once the latter function is known, numerical integration was used to calculate the various moments of the distribution and perform further characterization of the reactor.

6. Models for Non-ideal Reactors

To further characterize the performance of tubular reactors/contactors equipped with screen-type static mixers by means of the residence time theory, the commonly used one parameter model, namely the axial dispersion model was employed in this investigation. This model is used when small deviations from ideal plug flow exist, and under such conditions, it should render comparable residence time distribution function, $E(t)$ to the other commonly used tanks-in-series model (Fogler, 1999; Levenspiel, 1972). The theory and mathematics behind this model is mature and thoroughly explained in reactor design textbooks. Consequently it will only be briefly presented here.

a. Axial dispersion model

This model considers the flow inside the reactor to be plug flow on top of which is superimposed a certain degree of backmixing, the magnitude of which is independent of position in the vessel (Levenspiel, 1972). Because the material flowing inside the reactor/contactor is continuously redistributed by means of eddies, these disturbances can be calculated by analogy to molecular diffusion and can be written as shown in Equation (11),

$$\frac{\partial C}{\partial t} = D_{ax} \cdot \frac{\partial^2 C}{\partial z^2} - \frac{\partial (UC)}{\partial z} \tag{11}$$

where C is the concentration of the tracer and D_{ax}, is the longitudinal or axial dispersion coefficient, which characterizes the degree of backmixing in the reactor (Fogler, 1999; Levenspiel, 1972). The solution of this model relies on the boundary conditions and involves the dimensionless Peclet number, Pe; which for tube flow is defined as

$Pe = L \cdot U / D_{ax}$, where L is the mixing chamber length, and U is the mean flow velocity.

Because the tracer injection will be treated as an imperfect pulse with a certain distribution when entering the mixing section, the uniformly open system boundary conditions will be assumed in the current study. Under such conditions, the solution to Equation (11) assumes the following form for the residence time distribution function (Fogler, 1999; Nauman, 2008).

$$E(\Theta) = \tau E(t) = \frac{1}{2} \cdot \sqrt{\frac{Pe}{\pi \cdot \Theta}} \cdot \exp\left(-\frac{Pe \cdot (1-\Theta)^2}{4 \cdot \Theta} \right) \tag{12}$$

where Θ is the dimensionless time, $\Theta = t/\tau$.

The mean residence time of this distribution is given as $t_m = \tau \cdot (1 + 2/Pe)$. However, the value of Pe can be calculated by solving the relationship that relates the mean residence time and variance of the impulse response function, $E(t)$, with Pe, according to Equation (13).

$$\frac{\sigma^2}{t_m^2} = \frac{2Pe + 8}{Pe^2 + 4Pe + 4} \tag{13}$$

C. Results and Discussion

In this investigation, various operational parameters, as well as reactor/contactor design geometries, were varied with the objective of identifying their effect on the residence time distribution, specifically on the axial dispersion coefficient. Hydrodynamic studies related to pressure drop requirements to drive the flow inside tubular contactors equipped with screen-type static mixers were also performed and the results are reported in the following sections.

1. Pressure Drop Experiments

An important characteristic of static mixers is the generation of high pressure drop when compared to flow in empty pipe. For the purpose of comparison between several types of static mixers, pressure drop has also been reported by means of the *Z*-factor, the Newton number, Ne, or the Fanning friction factor, $f/2$ (Kumar et al., 2008; Li et al., 1997; Theron et al., 2010; Theron and Le Sauze, 2011). While the Newton number and the friction factor are directly related to each other following Equation (14), the *Z* factor is the ratio of the pressure drop across the mixer to that across the same pipe without static mixing elements, as shown in Equation (15).

$$Ne = 2 \cdot f = \frac{\Delta P \cdot D}{L \cdot \rho \cdot U^2} \tag{14}$$

$$Z = \frac{\Delta P_{\text{with static mixers}}}{\Delta P_{\text{empty pipe}}} \tag{15}$$

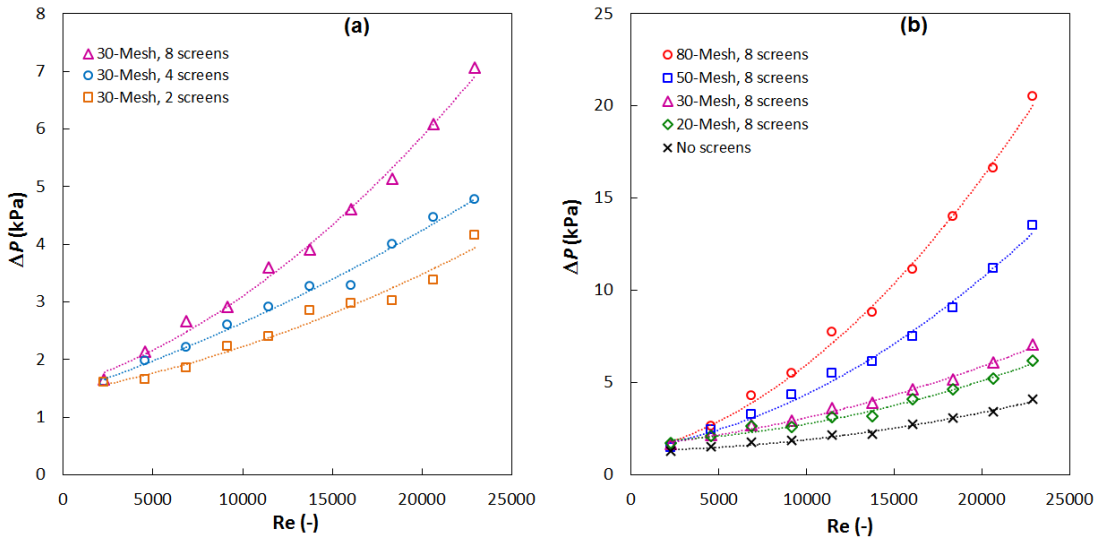

Figure 4: Pressure drop across the mixer length, (a) effect of number of elements; (b) effect of screen geometry

Figure 4a shows the effect of varying the number of elements on the pressure drop in the system for the case of 30-mesh screens. It is evident that a larger number of screen elements in the pipe produce a larger ΔP, an expected result. Furthermore, the effect of varying the screen geometry on the pressure drop in the system is depicted in Figure 4a, where an increase in the mesh number increases ΔP. This could not be explained only by relating the pressure drop to the mesh open area since the 80-mesh and 50-mesh screens have comparable screen open areas (31.4% and 30.3%, respectively), however, it appears that the pressure drop is also a direct function of the mesh opening ($M - b$), which decreases with an increase in the mesh number (Table 1). This is evident from the correlation of ΔP, for all screens, depicted in Equation (16) with its parity plot shown in Figure 5.

$$\Delta P\left(kPa\right) = 0.004 \cdot \mathrm{Re}^{0.805} \cdot \alpha^{0.397} \cdot \left(M - b\right)^{-0.612} \qquad \left(R^2 = 0.905\right) \qquad (16)$$

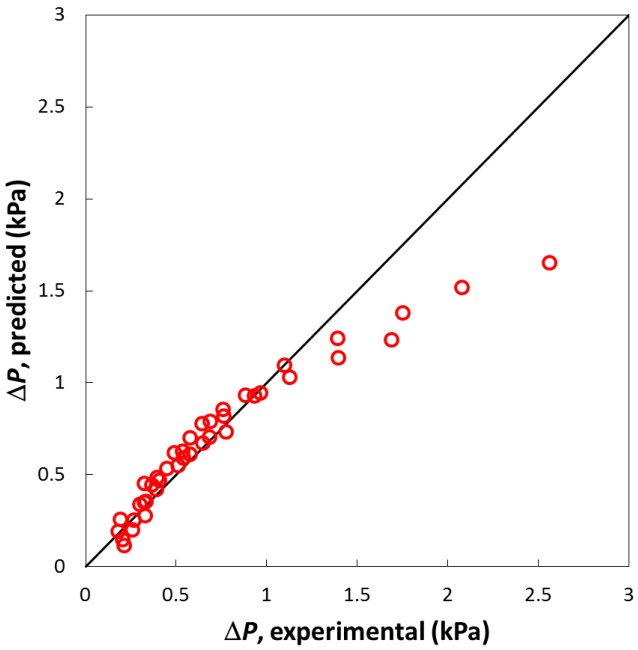

Figure 5: Parity plot of the correlated versus the experimental pressure drop for all screen geometries

It should be noted that a better regression line can be obtained using a different correlation type (cf. appendix), however this work was presented to keep conformity with most studies where the pressure drop is correlated in the form $\Delta P \propto \mathrm{Re}^{p}$.

Moreover, the effect of varying the flow velocity on the friction factor, *f/2*, is reported in Figure 6a. It is evident that the friction factor decreases almost linearly with increasing the flow rate through the mixer while it starts plateauing at higher Re (> 20,000) similarly to the behavior in empty pipe. In order to account for the varying porosities of static mixers, many investigators (Kumar et al., 2008; Li et al., 1997; Theron et al., 2010; Theron and Sauze, 2011) suggest the use of interstitial velocities while calculating the friction factor and Re. In such cases, the effective velocity term is that through the openings of the static mixer (which can be looked at as a combination of orifices) rather than the interfacial velocity in the open pipe. Under such conditions, the interstitial friction factor becomes equal to,

$$\frac{f_i}{2} = \frac{\Delta P \cdot D \cdot \alpha^2}{4 \cdot L \cdot \rho \cdot U^2} \tag{17}$$

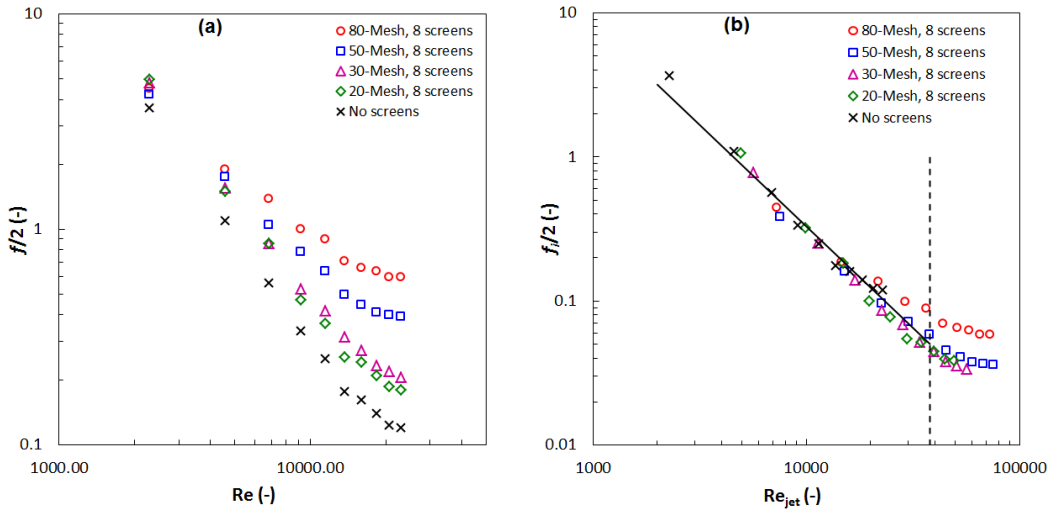

Figure 6: Effect of (a) Reynolds number on the friction factor, and (b) Re_{jet} on the interstitial friction factor, $f_i/2$.

where, α is the fraction open area of the screen. Similarly, the Reynolds number will also be calculated based on the interstitial velocity, where in this case, it is commonly known as the macroscopic jet Reynolds number, Re_{jet}.

$$\mathrm{Re}_{jet} = \frac{D \cdot U \cdot \rho}{\mu \cdot \alpha} \tag{18}$$

Figure 6b shows the effect of accounting for the interstitial velocity through the screen mixers on the friction factor. It is very clear that regardless of the screen geometry, $f_i/2$ values overlap until a critical Re_{jet} is reached, the value of which appears to be dependent on the screen geometry, where $f_i/2 \propto \mathrm{Re}_{jet}^{-1.4}$ (with $R^2 = 0.967$, for Re_{jet} < 38,000 which is highlighted on Figure 6b).

Finally, the values of the Z factor in the current investigation were found to be much smaller than those reported in the literature for other types of static mixers. Figure 7 shows the variation of the Z factor with the pipe Reynolds number, where it is very clear that the value of Z is a direct function of the screen geometry, with higher values

of *Z* for higher mesh numbers. While *Z* plateaus at close to unity for large mesh openings, this value reaches a maximum of approximately 5 for the smallest mesh opening at relatively high Re (~ 23,000). These values compare very favorably with those reported for other types of static mixers (e.g. Kenics, SMX, Lightnin, Komax, etc…), where the value of *Z* varies between 5.5 and 300 for the laminar flow regime only, with its value expected to increase rapidly to several hundred at higher Re (Thakur et al., 2003). Comprehensive summaries of *Z* values for mostly laminar flows are tabulated in the works of (Kumar et al., 2008; Theron and Sauze, 2011). This clearly highlights the fact that screen-type static mixers are more energy efficient when compared to other static mixers.

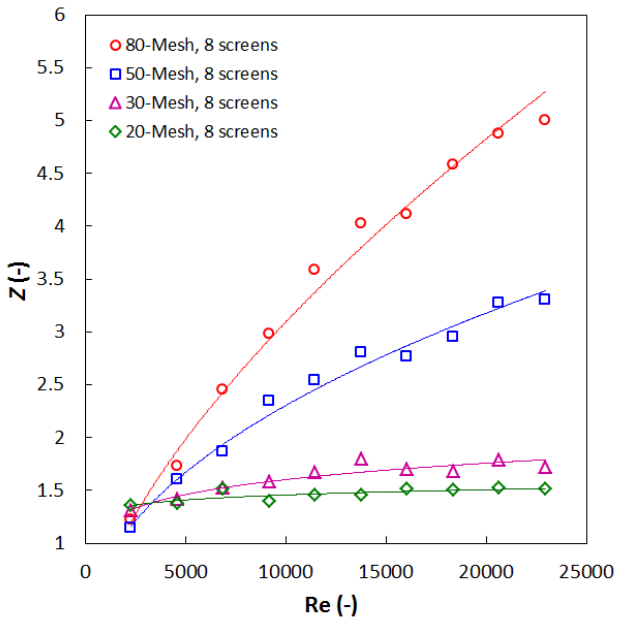

Figure 7: Effect of Re on the value of the *Z* factor.

2. RTD experiments

As previously stated, KCl was used to perform RTD experiments because the linear relationship between its conductivity and concentration in the range of investigated conditions. While the injected tracer was sent into the system in a very short period of time, the analysis adopted in the current work assumes an imperfect

pulse condition and therefore recordings of both the inlet and outlet conductivities were performed at all times.

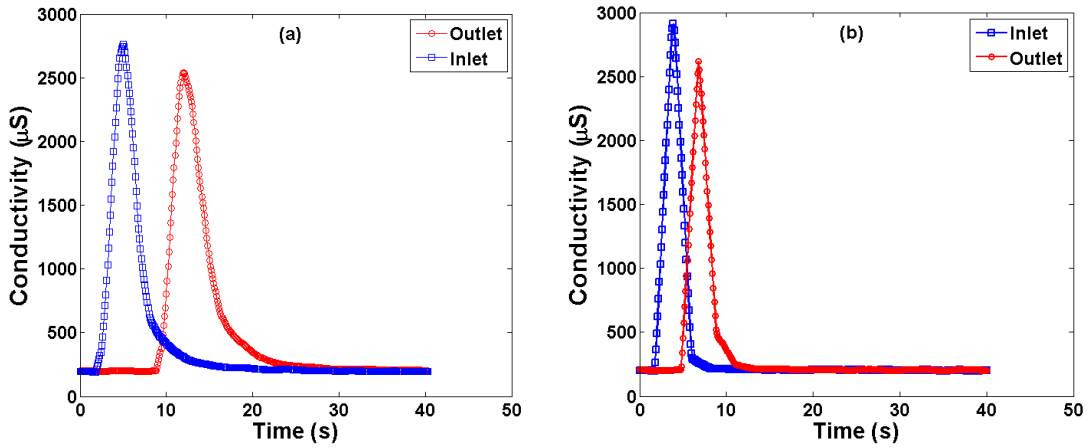

Figure 8: Raw conductivity data under different operating and design conditions, (a) Q = 4 L/min, N = 0; (b) Q = 12 L/min, 50-mesh, N = 2.

A sample of the raw data obtained in a given experiment is shown in Figure 8, where the "background" conductivity of RO water appears in the dataset. In addition, the effect of flow velocity on the inlet and outlet conductivity distributions can be clearly discerned in Figure 8b. At higher velocities the liquid volume containing the tracer is expected to spend a shorter time around the sensor, which translates into a narrower distribution of electrical conductivity at either the inlet or outlet of the mixing zone. Moreover, because the residence time in the system is shorter, the outlet conductivity distribution is closer to the inlet distribution. All these phenomena are clearly illustrated in Figure 8b when compared to Figure 8a. The raw conductivity data is then converted into normalized concentrations (shown in Figure 9) in order to perform the necessary RTD calculations. The normalized concentrations would have an adjusted baseline at C = 0 which replaces the "background noise" (conductivity of RO water). It should be noted that by normalizing the concentrations, the shape of the distributions was not affected.

All experimental runs were conducted a minimum of three times to ensure repeatability of the results. In addition, a mass balance was conducted on each of these runs to check if the two sensors are measuring a comparable amount of salt (mass conservation) in the system and it was found that the difference between the inlet and outlet recorded amounts of KCl varied by 11.7% on average.

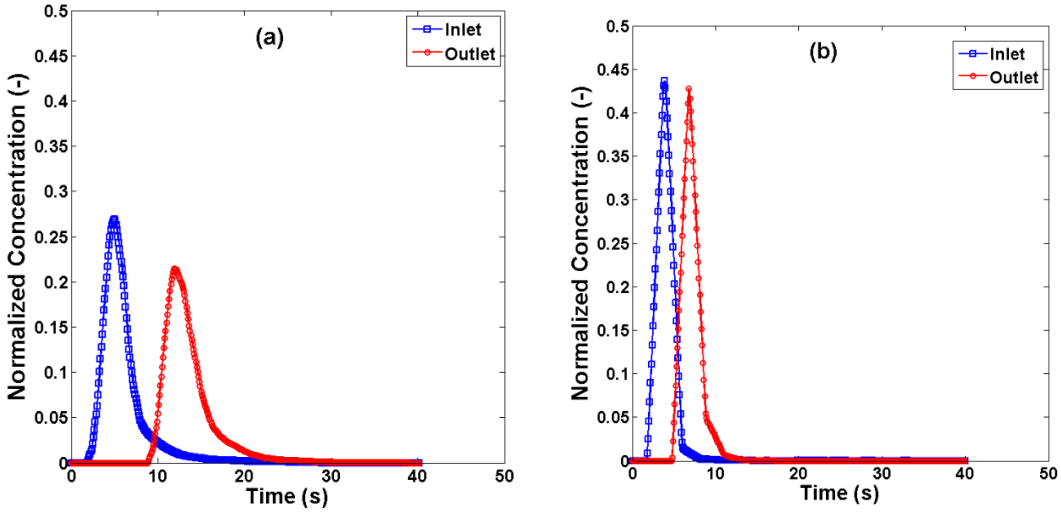

Figure 9: Normalized concentration under different operating and design conditions, (a) Q = 4 L/min, N = 0; (b) Q = 12 L/min, 50-mesh, N = 2.

a. Selection of the fitting parameter

An in-house computational subroutine to find the best fitting parameter was executed in MatLab® on each run in order to find the residence time distribution function, $E(t)$, which would be used in analyzing the system. In addition to the aforementioned conditions of the conservation of the first and second moments of the distribution while searching for the best fitting parameter, γ, an additional criterion was introduced in this work. This relied on calculating γ that returns the distribution with the minimum fluctuations in the time domain. Mao et al., (1998) discussed this issue and highlighted the fact that the RTD obtained using the Mills and Dudukovic, (1989) algorithm requires additional smoothing in the time-domain where negative peaks of no

physical significance can appear after applying the inverse Fourier transform to $\tilde{E}(\omega)$. In order to eliminate such peaks of no significance, the computed $\underline{E}(t)$ function was fitted with a Gaussian distribution in the time domain. Such undertaking is justified by the fact that almost all impulse responses showed a Gaussian behavior as shown in Figure 10.

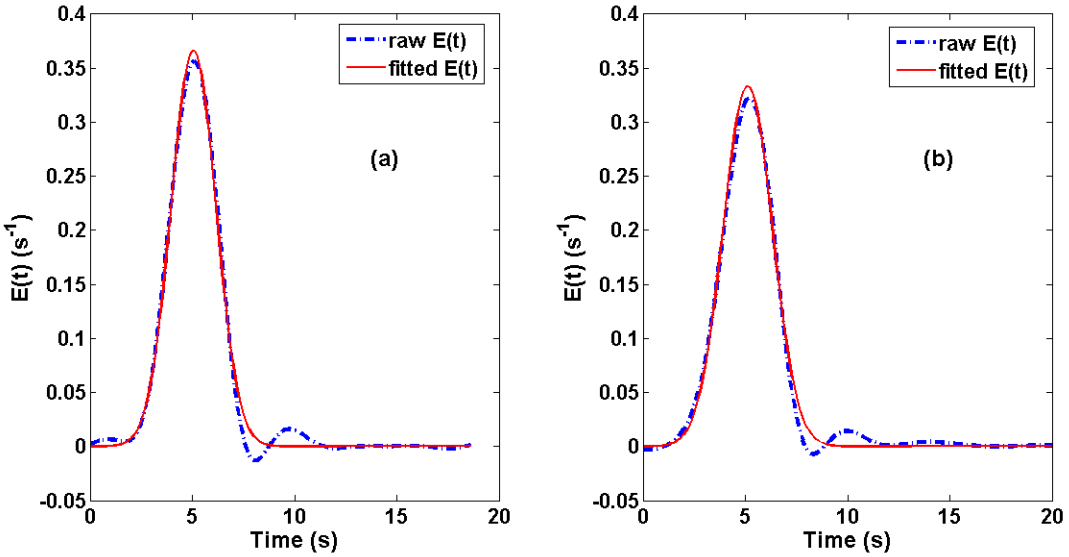

Figure 10: Plot of the "raw" impulse response, $E(t)$, and its Gaussian fit; (a) $N = 1$, 20-mesh, Re = 3,450; (b) $N = 4$, 50-mesh, Re = 4,600.

Further validation of this approach was concluded by checking the convolution of the inlet concentration measurements and the computed impulse response, according to Equation (6), which should render the measured outlet concentration. Figure 11(a–d) show the result of the convolution integral for various reactor/contactor designs and operating conditions, plotted against the normalized outlet concentrations. It is very clear that the computed RTD renders an exact description of the macromixing behavior of the system since all distributions obtained by the convolution integral fit very well the measured data.

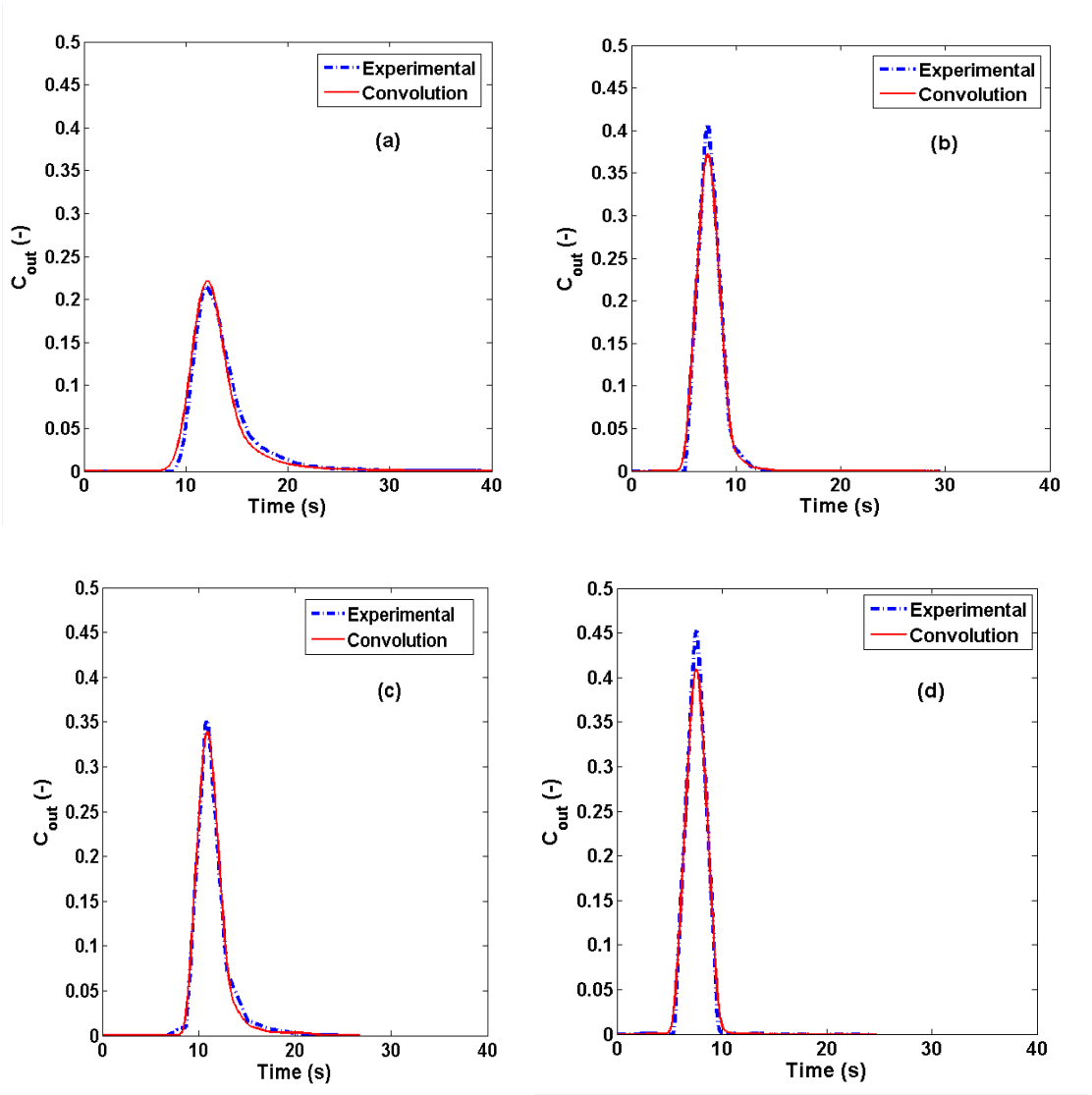

Figure 11: Normalized outlet concentration, experimental vs. convolution of inlet concentration and impulse response; a) $N = 0$, Re = 2,300; b) $N = 2$, 20-mesh, Re = 6,900; c) $N = 4$, 50-mesh, Re = 3,450; d) $N = 8$, 30-mesh, Re = 11,500.

b. Mean residence time

A major use of the RTD analysis is to determine whether or not there exist dead volumes or bypassing in the reactor/contactor under investigation. For this purpose, the mean residence time, t_m, computed from the RTD experiments using Equation (3) is compared with the theoretical residence time, $\left(\tau = V/Q\right)$ in Figure 12. If a dead (or stagnant) volume exists in the mixing zone, t_m is expected to be smaller than τ because the flow would have a smaller volume to sweep and would therefore exit

faster. The situation is inverted in the case of bypassing or channeling, where a larger t_m would be expected since part of the flow would immediately exit the system leaving a smaller effective flow rate to sweep the system (Fogler, 1999; Levenspiel, 1972b). It is obvious from Figure 12, where all 119 experimental points are plotted, that the data is scattered around the theoretical value, with an average relative error of 8.4%, which indicates the absence of dead volumes or channeling in the system. The discrepancy between the data around the lowest superficial velocity can be attributed to a lower accuracy of the flow meter at those flow rates; nonetheless, the data will be presented as if it were exactly at that flow rate.

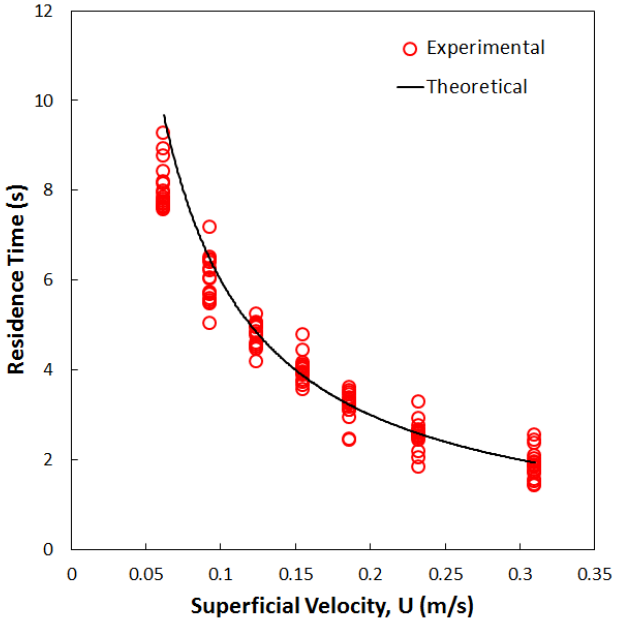

Figure 12: Comparison between mean (from RTD), t_m, and theoretical, τ, residence times in the mixing zone for all 119 experimental runs.

c. Effect of flow velocity on RTD

At higher flow rates, the residence time inside the mixing zone becomes smaller rendering a narrower $E(t)$ distribution that is shifted towards shorter time values. This is clearly observed in Figure 13a where $E(t)$ is plotted for various flow rates in the same reactor configuration. However, the situation becomes different when

dimensionless time, Θ, is used in order to normalize all distributions. In such cases, it becomes very clear that the dimensionless distribution $E(\Theta)$ becomes broader with an increase in the flow velocity (Figure 13b). This reflects an increase in the axial dispersion in the system with an increase in the flow velocity.

Using the one parameter model, presented in Equation (12), the Péclet number, Pe, can be computed by fitting the equation to the computed $E(\Theta)$. The value of Pe was found to decrease with an increase in the flow rate, with its value being a direct function of the reactor geometry (Figure 14a).

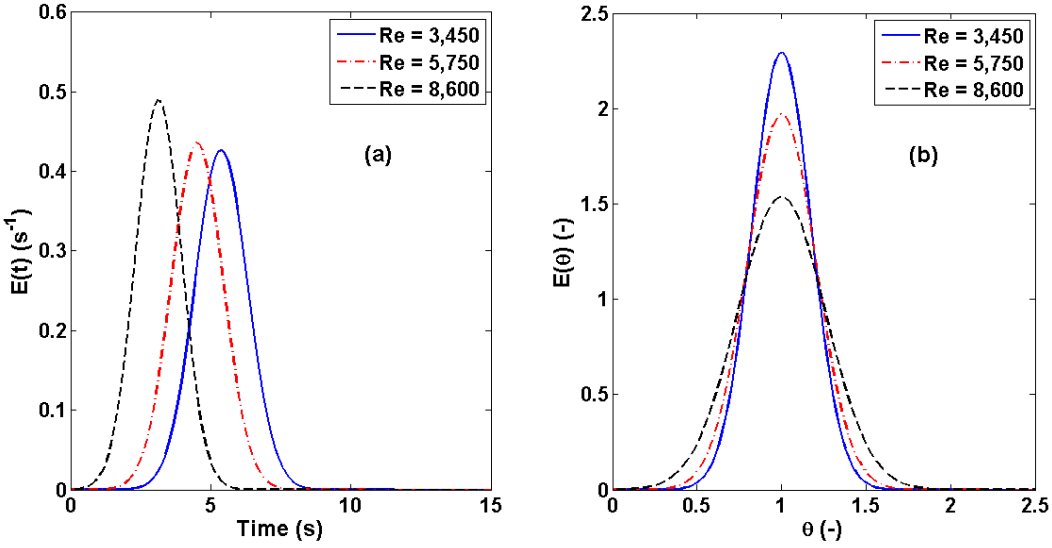

Figure 13: Effect of flow velocity on $E(t)$ and $E(\theta)$; ($N = 2$, 30-mesh).

This is attributed to an increase in the axial dispersion coefficient as the velocity increases. Further, the flow in an empty pipe showed a lower value of Pe when compared to the reactor equipped with screen-type static mixers.

Similar behavior is also observed when comparing the coefficient of variation along the length of the reactor. The COV was found to increase with an increase in the velocity with the values computed for pipes equipped with screen mixers being constantly smaller than those of an empty pipe.

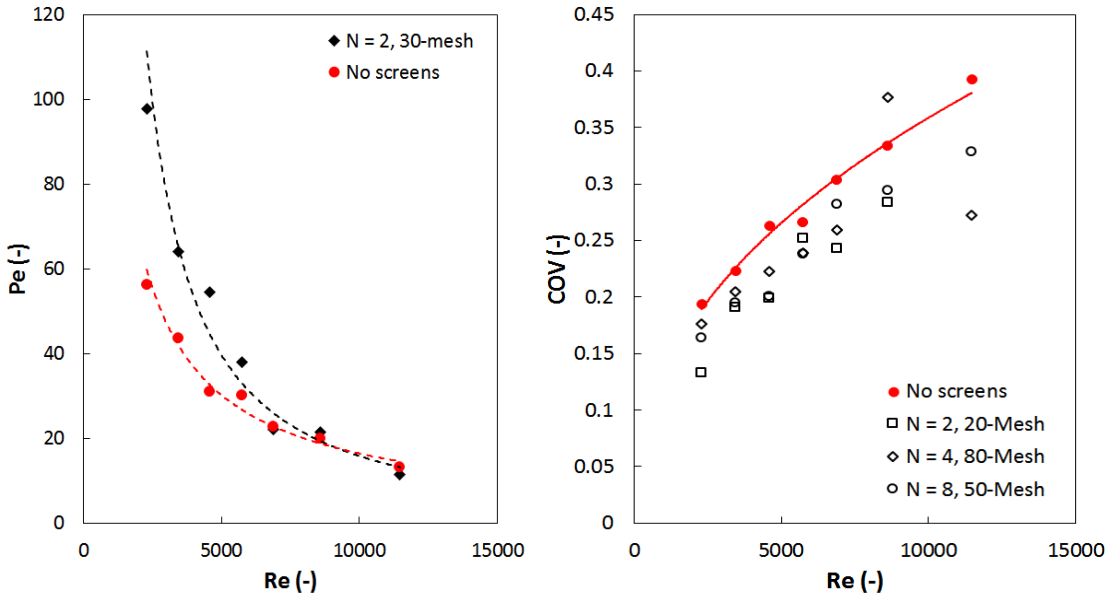

Figure 14: Effect of increasing the flow velocity on Pe and COV

This finding highlights the fact that the presence of screen-type static mixers better homogenize the flow under the same operating conditions when compared to an empty pipe configuration.

d. Effect of screen geometry and number of screens on RTD

To investigate the effect of varying the number of static mixer elements as well as their geometrical design on the macromixing behavior of the system, the axial dispersion coefficient was calculated from the Pe values. The effect of varying the screen geometry is shown in Figure 15a where the axial dispersion coefficient is plotted against the Reynolds number, and no clear effect could be discerned. Similarly, the effect of varying the number of screen elements inserted in the mixing zone is shown in Figure 15b. It was interesting to note that while the axial dispersion coefficient continuously increases with an increase in the flow velocity, no significant effect for the screen geometry and number of screens could be highlighted in such a comparison.

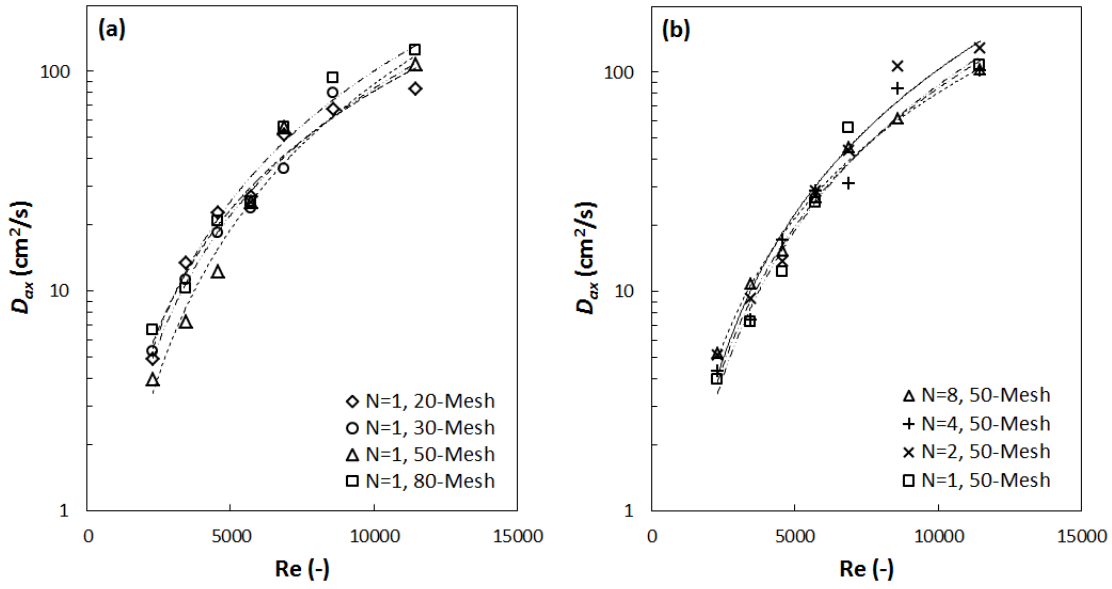

Figure 15: Effect of varying the design conditions on the axial dispersion coefficient: (a) effect of screen geometry; (b) effect of number of screens

The empty pipe Reynolds number, Re, measures the ratio of inertial to viscous forces in the system with the pipe diameter being the characteristic length. However, for flow through woven screens or grids, there exist several other characteristic lengths that could be employed when computing the Reynolds number, e.g. wire diameter, mesh opening, individual jet diameter, etc… While no agreement on which characteristic length to be used is available in the literature, the wire diameter remains a commonly acceptable length when investigating the turbulence of the flow through screens but the mesh size remains the most commonly employed length. In the latter case, the corresponding Re is called the mesh Reynolds number, Re_M, and defined according to Equation (19).

$$\mathrm{Re}_M = \frac{M \cdot U \cdot \rho}{\mu} \tag{19}$$

It is therefore interesting to note that when the axial dispersion coefficient is plotted against Re_M, a clear effect of the screen geometry is observed where screens with the smallest mesh size, M, i.e. 80-mesh, exhibiting the largest overall axial

dispersion (Figure 16). Based on this dimensionless group, the larger the mesh opening, the smaller is the axial dispersion coefficient. However, such conclusion can be overturned by changing the dimensionless group where the effect against the macroscopic jet Reynolds number (defined in Equation (18)) shows that the smaller the screen open area, α, the lower is D_{ax} (Figure 17) with screens of close open areas (i.e. 50- and 80-mesh) rendering almost an identical performance with larger number of screen elements inserted in the pipe.

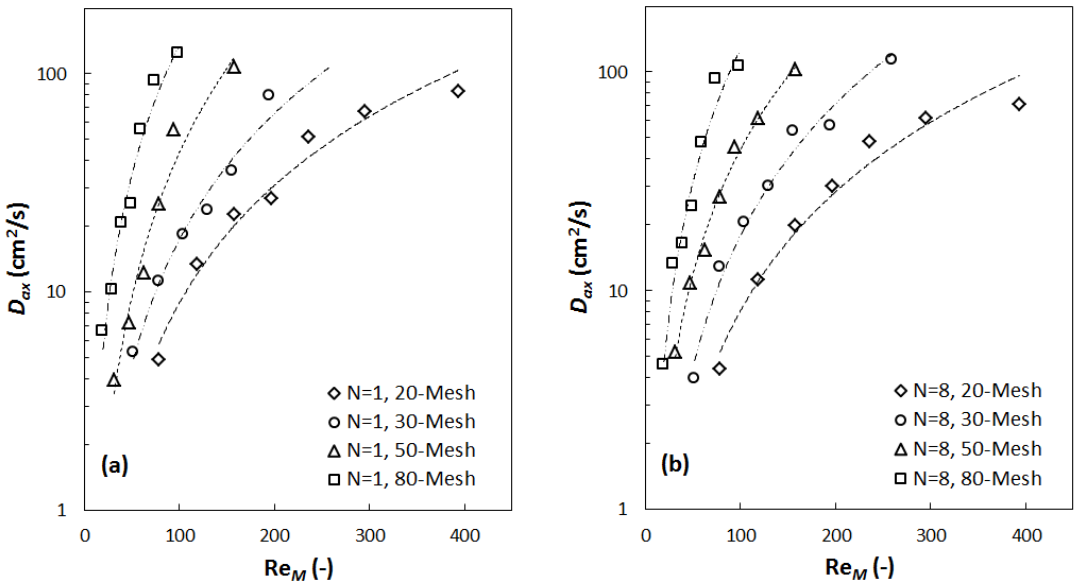

Figure 16: Effect of screen geometry on the axial dispersion coefficient with respect to the mesh Reynolds number, Re_M: (a) $N = 1$, (b) $N = 8$.

While such conclusions might appear contradictory, it is not, and the choice of the characteristic length to compute the Reynolds number remains an important criterion to judge the performance of the mixer and design it accordingly.

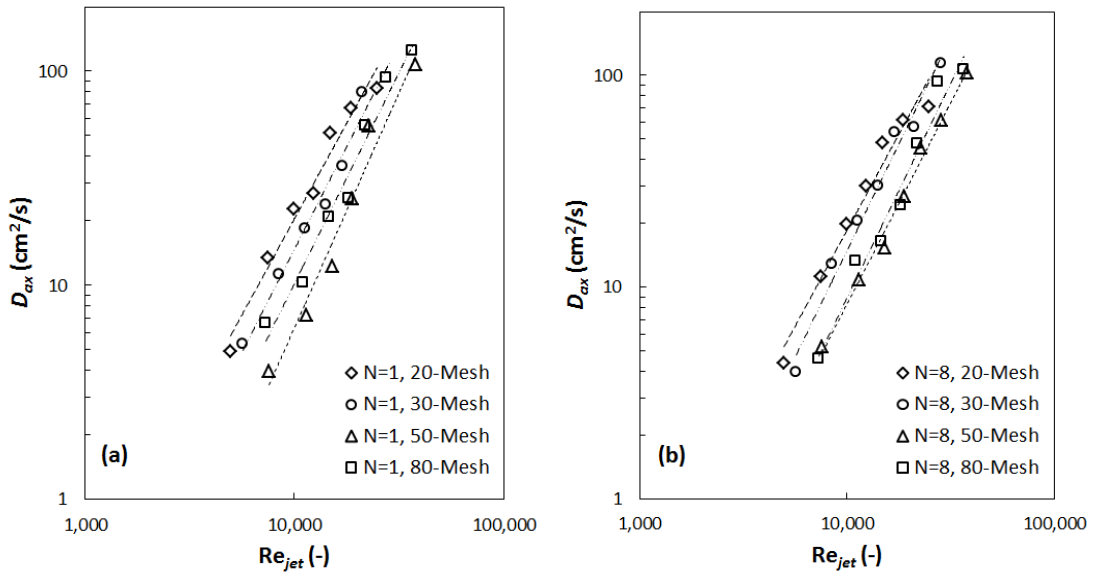

Figure 17: Effect of screen geometry on the axial dispersion coefficient with respect to the macroscopic jet Reynolds number, Re_{jet}: (a) $N = 1$, (b) $N = 8$.

Furthermore, no matter what is the choice of the Reynolds number, whether it is based on the macroscopic jet velocity or the mesh size or the empty pipe diameter, the effect of number of screen elements in the mixing zone remains negligible.

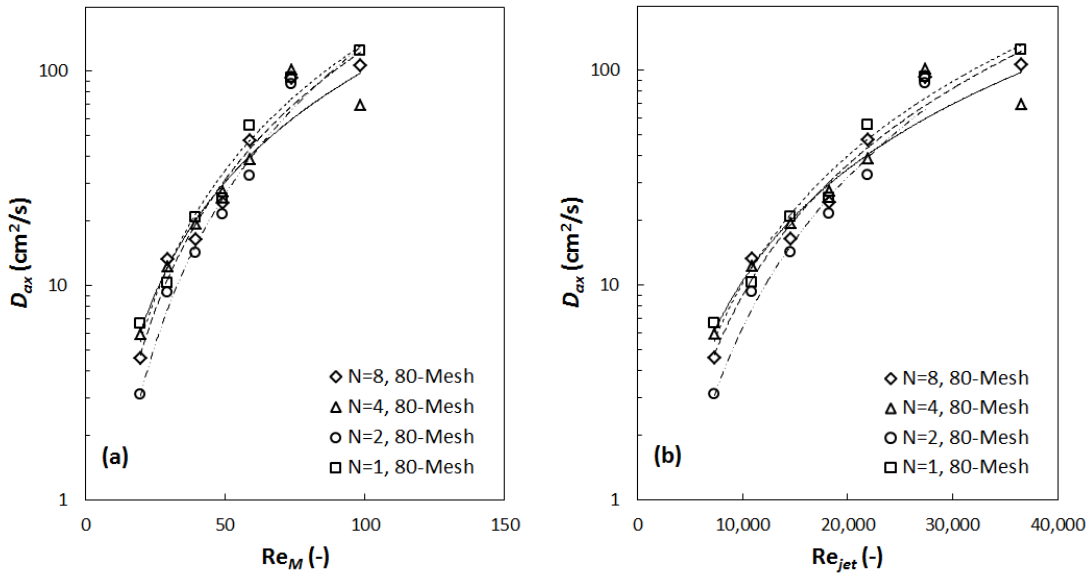

Figure 18: Effect of number of screens of the axial dispersion coefficient with respect to (a) the mesh Reynolds number, Re_M; and (b) macroscopic jet Reynolds number, Re_{jet}.

Figure 18(a) and (b) show the axial dispersion coefficient plotted against Re_M and Re_{jet} for different number of mixing elements of the same geometry. While it is

very clear that a scatter exists, and as will be shown in the next section, this parameter was found to have a minor effect on the exponent of the respective Re numbers with no major statistical significance.

e. Comparison with flow in an empty pipe and regression analysis

The advantages of utilizing screen-type static mixers are highlighted in Figure 19, which shows the calculated axial dispersion coefficient for all experimental runs plotted against those for the runs where no static mixers were inserted in the pipe. When all the parameters are lumped together (i.e. number of screen elements, screen geometry, and flow velocity) it is very evident that screen-type static mixers allow for a smaller axial dispersion when compared to an empty pipe and therefore a better mixing performance.

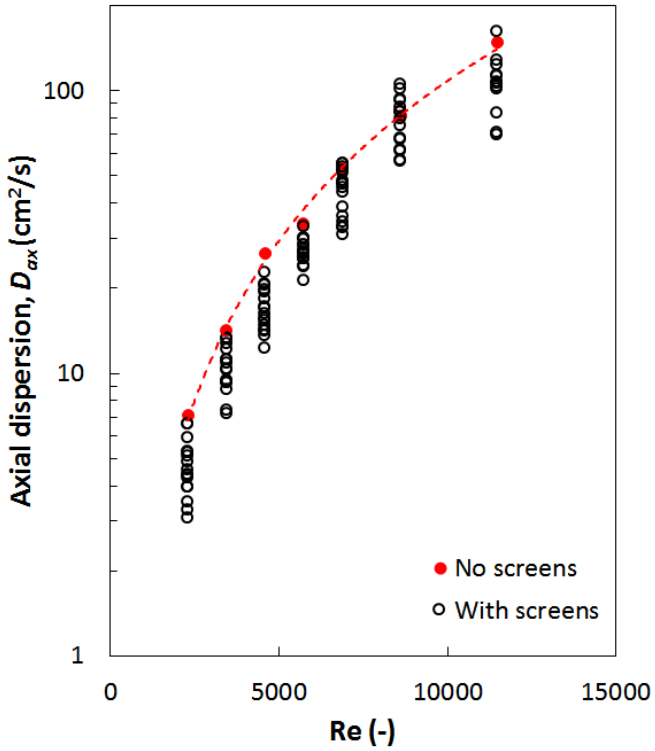

Figure 19: Comparison between the axial dispersion in the presence of screens with that for an empty pipe when plotted against the empty pipe Reynolds number, Re.

To the authors' knowledge, no such data or information is reported for other types of motionless mixers at such high Re values so it can be used for comparison between the mixers.

The data obtained in the current work were then correlated in order to be able to predict the performance of the mixer. The most significant parameters that played a role were found to be Re_{jet}, Re_M, and $(M–b)$. This is clearly highlighted in Equation (20) which predicts the value of the axial dispersion coefficient in the presence of screen elements only. The regression line ($R^2 = 0.991$) was found to predict quite well the experimental results as shown in the parity plot presented in Figure 20.

$$D_{ax}\left(\mathrm{cm}^2/\mathrm{s}\right) = \exp\left(-0.12N\right) \times \mathrm{Re}_M^{-0.43\sqrt{N}-2.61} \times \mathrm{Re}_{jet}^{(0.018N+4.543)} \times \left(M-b\right)^{3.61} \quad (20)$$

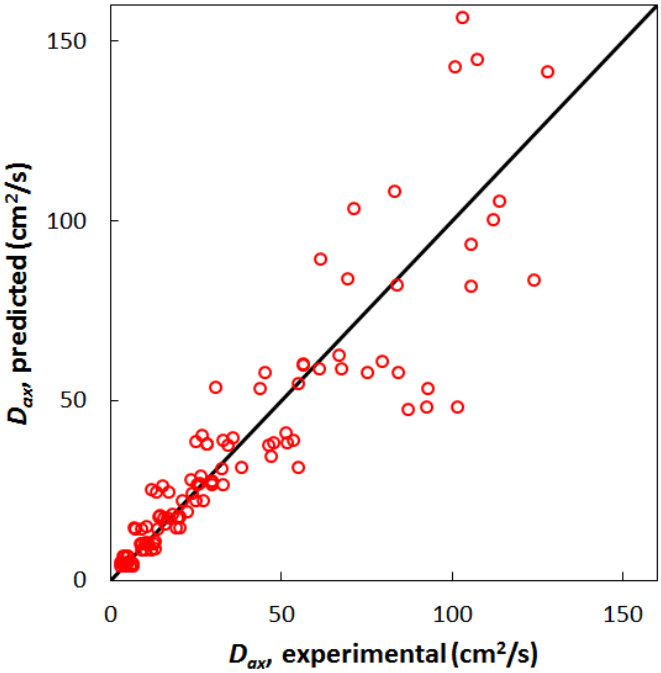

Figure 20: Parity plot for the predicted vs. experimental axial dispersion coefficient values

D. Conclusions

This study investigates the hydrodynamics and residence time distribution of one phase flow in tubular reactors/contactors equipped with screen-type static mixers. The measured pressure drop through various screen geometries and under different operating conditions was found to be a direct function of their mesh opening and screen fraction open area. From an energy efficiency perspective, screen mixers compared favorably with other types of static mixers, where the *Z* factor was found about two-orders of magnitude lower than values reported in the open literature for other types of motionless mixers. Furthermore, it was found that the axial dispersion coefficient in reactors equipped with screen mixers increases with an increasing flow velocity. However, the data could be interpreted in terms of various Reynolds numbers, depending on the characteristic length used. While the axial dispersion decreases with an increasing mesh size when compared on a mesh Reynolds number basis, the same data show that the dispersion decreases with the fraction open area of the screen when compared on the basis of Re_{jet}. Such a conclusion is therefore left to the user to decide on which characteristic length is more important for its application. In addition, while its effect is somewhat evident, no statistical significance was found for the effect of number of screen elements in the pipe on the axial dispersion coefficient, in this study.

CHAPTER II

Liquid-Phase Axial Dispersion and Hydrodynamics of Turbulent Gas-Liquid Co-Current Flows through Screen-type Static Mixers

A. Introduction

Static mixers are becoming indispensable in the process industry and their application for process intensification purposes is quickly gaining momentum (Al Taweel et al., 2013; Ghanem et al., 2014). This is driven by their intrinsic capability of achieving higher mass transfer and heat addition/removal rates when compared to traditional contactors/reactors, at lower capital and operating costs while also handling large flow rates (Al Taweel et al., 2013; Ghanem et al., 2014; Madhuranthakam et al., 2009; Peschel et al., 2012; Thakur et al., 2003). Other advantages include a smaller space requirement, higher reaction rates, optimal selectivity, lower by-product formation, reduced waste generation and enhanced operation safety.

A wide array of static mixers is commercially available in a variety of geometries, however, a common feature of these mixers is that turbulence is continuously produced and dissipated along the reactor length while redistributing the fluid transversely to the main flow with the only energy cost being a function of the pressure drop which dictates the power required for pumping (Ghanem et al., 2014; Lobry et al., 2011; Thakur et al., 2003). Studies available in the open literature investigated topics ranging from hydrodynamics of flow to rates of heat and mass transfer or competitive reactions and selectivity, in single- and/or multi-phase flow (Theron et al., 2010; Keshav et al., 2008; Li et al.,1997; Theron and Sauze, 2011a, 2011b; Ziolkowski and Morawski, 1987), highlight the abundance of numerical and experimental investigations that have been performed on various types (e.g. Kenics, Sulzer SMX and SMV, Lightnin, etc…).

One variant of these mixers, the screen-type static mixer (STSM), or woven wire mesh, is used to repetitively superimpose an adjustable, radially-uniform, highly-turbulent field on the nearly plug flow conditions encountered in high velocity pipe

flows (Al Taweel et al., 2005, 2007, 2013; Azizi and Al Taweel, 2007, 2011a, 2011b). The very high energy dissipation rates generated in the thin region adjacent to the STSM as well as the quasi-isotropic turbulence further downstream, proved to be very effective in processing multiphase systems (Al Taweel et al., 2005, 2007, 2013; Azizi and Al Taweel, 2007; Azizi and Taweel, 2011a; Al Taweel and Chen, 1996) and studying the effect of turbulent mixing on the evolution of chemical reactions as well as testing the applicability of micro-mixing models (Bennani et al., 1985; Bourne and Lips, 1991).

The ability of STSM to promote contact between different phases was found to be about 5-fold more energy efficient than mechanically agitated tanks equipped with Rushton-type impellers (Al Taweel and Chen, 1996). Furthermore, interfacial areas as high as 2,200 m^2/m^3 could be efficiently generated in the case of gas-liquid systems (Chen, 1996), while oxygen transfer efficiencies as high as 4.2 kg/kWh, were achieved even in the presence of surfactants (Al Taweel et al., 2005). For the case of liquid-liquid dispersions, volumetric mass transfer coefficients, $k_L a$, as high as 13 s^{-1} were attained and enabled for 99% of the equilibrium conditions to be achieved in less than 1 s (Al Taweel et al., 2007).

The aforementioned good performance of screen-type static mixers, however, is directly related to the mixer (screen) geometry, reactor configuration, and/or the operating conditions, where any modification in these parameters will directly impact the efficiency of the reactor by affecting the extent of micro-, meso- and macro-mixing as well as the pressure drop across the mixer. Characterizing mixing and hydrodynamics of the flow is therefore of paramount importance for various economic and environmental considerations as they govern the process efficiency.

For the case of STSM, the hydrodynamics and residence time distribution (RTD) of single phase flow were investigated in a previous study (Abou Hweij and Azizi, 2015). The study focused on the effect of number of mixing elements, inter-screen spacing, screen geometry/design, and flow velocities on the pressure drop and axial dispersion in the reactor. It was found that screen mixers compared favourably with other types of static mixers from an energy efficiency point of view (i.e. pressure drop measurements), and that the axial dispersion coefficient increased with an increasing flow velocity while always remaining lower than that measured for empty pipes. The definition of the characteristic length for Reynolds number calculation also proved to be an import criterion in characterizing macro-mixing in the case of STSM. For example, an increase in the mesh Reynolds number (calculated based on the mesh size of the screen) reflected a decrease in the axial dispersion coefficient, while the same data showed a decrease in axial dispersion with a reduction in the jet Reynolds number (calculated based on the fraction open area of the screen) (Abou Hweij and Azizi, 2015). No data pertaining to the presence of a second phase on either the pressure drop and/or axial mixing was reported in that investigation.

Consequently, the objectives of this study are to investigate the hydrodynamics and macro-mixing (in terms of RTD measurements) in turbulently flowing gas-liquid dispersions through STSM. In particular, the investigation will focus on the effect of adding a second phase on the pressure drop as well as the liquid-phase axial dispersion coefficient over a wide range of operating and design conditions. The results of this study will therefore be of great importance in reaching optimal designs based on macromixing patterns for multiphase tubular reactors/contactors equipped with STSM.

B. Materials and Methods

1. Experimental Setup

In a similar fashion to the earlier work (Abou Hweij and Azizi, 2015) a pulse injection of a highly concentrated aqueous salt solution was used to measure the RTD in the reactor/contactor by means of measuring the changes in electrical conductivity in reverse osmosis (RO) water of low initial conductivity. The analysis was performed assuming an imperfect pulse technique, which was accomplished by measuring the electrical conductivity at both entrance and exit to the mixing section.

The continuous flow experimental setup used in the present investigation is a minor modification of the setup used in the previous study (Abou Hweij and Azizi, 2015). The modified setup which is schematically depicted in Figure 21 has been adjusted to allow for the injection of a secondary gaseous phase to the primary aqueous phase.

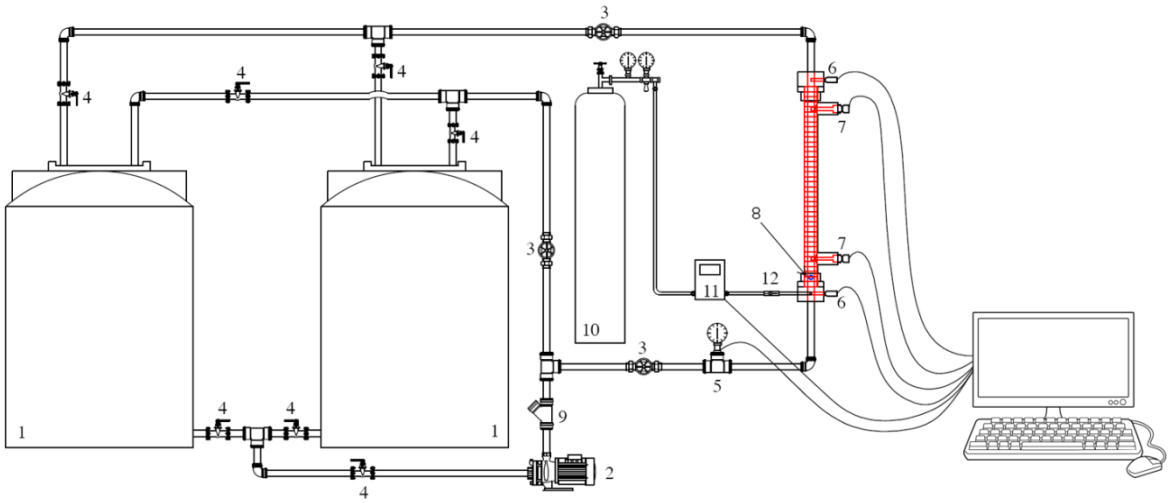

Figure 21: Schematic representation of the experimental setup (1) Supply/Drain tank, (2) centrifugal pump, (3) gate valve, (4) ball valve, (5) flow meter, (6) pressure sensors, (7) conductivity sensors, (8) tracer injection port, (9) check valve, (10) compressed gas cylinder, (11) mass flow controller, (12) ball valve.

Reverse osmosis (RO) water was collected in a 500 L tank from which it was fed to the static mixer loop using a constant speed centrifugal pump (Pedrollo, model PKm80) . The manually regulated flow rate of water entering the mixing section was measured by means of a digital flow meter (Omega model: FP7002A) while the gas flow was controlled automatically by means of a mass flow controller (Omega model: FMA 8311). Liquid flow rate varied between 30 and 45 L/min at intervals of 5 L/min while the gas flow rates ranged between 3 and 6 L/min at intervals of 1 L/min. These provided a large range of experimental conditions over which the RTD experiments were performed, additionally, they allowed for testing the effect of varying the gas flow rate incrementally. However, for the pressure drop studies, the effect of changing the dispersed phase volume fraction, ϕ, at equal specific intervals over a wider range of flow rates was studied. The pressure at the inlet and outlet of the mixing section was recorded while changing the gas holdup between 5%, 10% and 20%.

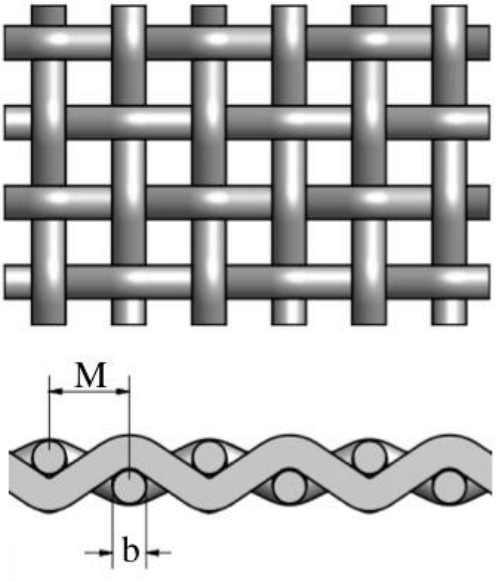

Figure 22: Geometry of the STSM

For detailed information about the experimental setup and its various constituents, the reader is referred to the work of Abou Hweij and Azizi (2015).

However, the effective diameter of the mixing section which contained a varying number of static elements is 37 mm with a total length of 600 mm. The setup was provided with an injection valve through which the tracer pulse was injected and conductivity measurements were taken at the inlet and outlet to the mixing section by means of two identical conductivity sensors (Omega model CDCE 90-X) placed at 75 and 675 mm from the injection point, respectively. Two pressure transducers (Siemens QBE2002-P1) were also fixed at the top and bottom of the reactor section, 855 mm apart. Data from all sensors was collected at a frequency of 10 Hz by means of a National Instruments data acquisition board (NI USB-6218) and a specially developed LabView program.

The effect of changing the screen geometry on the RTD was investigated for four different screen designs, the characteristics of which are presented in Table 3 and their geometry shown in Figure 2. It should be noted that the numerical value of the mesh number (cf. Table 3) indicates the number of meshes per linear inch (*i.e.* mesh number = 25.4/M –in mm–).

Mesh number, Mn	$M \times 10^3$ **(m)**	$b \times 10^3$ **(m)**	$(M - b) \times 10^3$ **(m)**	α **(%)**
20	1.27	0.4064	0.8636	46.2
30	0.8382	0.3048	0.5334	40.8
50	0.508	0.2286	0.2794	30.3
80	0.3175	0.1397	0.1778	31.4

Table 3 Characteristics of the investigated stainless steel STSM

Furthermore, three different reactor/contactor configurations were tested, where RTD measurements were taken in the presence of 4 or 8 STSM elements equidistantly placed in the mixing section in addition to the case where no elements were inserted. Moreover, the first screen element was held at 60 mm above the inlet conductivity sensor for the case when 8 screen elements were used and at 120 mm

above the sensor when 4 screens were used. Such a configuration ensured a proper distribution of the screens over the entire mixing section volume.

2. Experimental Method

Similarly to the work on single phase flow (Abou Hweij and Azizi, 2015), RTD measurements were performed by means of recording the electrical conductivity at the inlet and outlet of the reactor after imposing a pulse injection of a highly conductive salt solution in the low conductivity RO water (~ 200 μS) used in all experiments. RO water was always pumped from a clean supply tank and the outlet of the mixing section was directly drained or collected in a separate tank to ensure that no accumulation of salt occurs.

KCl was used as the tracer because of the linear relationship between its concentration and electrical conductivity. A stock solution of 0.9 mol/L was prepared using deionized water, from which 24.8 mL were repetitively injected in the system as a pulse disturbance. This volume was kept constant throughout the experiments by using the same injection syringe, and all injections were performed in less than 1 s. Depending on the operating conditions, this meant the maximum conductivity would range between 3,000 and 4,000 μS, which is substantially larger than the base conductivity of the water.

3. Methodology

Residence time studies follow a well-established, mature theory that has been gaining momentum since the 1950s with the pioneering work of Danckwerts (Danckwerts, 1953), even though his well-known axial dispersion model was developed by Langmuir (Langmuir, 1908; Nauman, 2008). In this theory, the response of the

system to a disturbance is analyzed to characterize the macro-mixing, and/or the flow, within it. Several articles and textbook chapters have been devoted to explaining this theory (Fogler, 1999; Levenspiel, 1972; Häfeli et al., 2013; Madhuranthakam et al., 2008; Din et al., 2008; Madhuranthakam, 2009), and therefore the reader is referred to these works to get familiarized with its concept and various parameters.

Because of the very short residence time of the flow in the mixing section under investigation in this work, which is in the order of 0.75 to 1.2 s, the tracer injection (performed in under 1 s) cannot be considered as a perfect pulse. Consequently, the experiments have to be analyzed by assuming an imperfect pulse technique. Under these conditions and knowing the inlet and outlet tracer concentrations, the system response, or the exit-age distribution function, $E(t)$, can be obtained by the deconvolution of these two signals.

4. RTD analysis and Deconvolution

The outlet concentration is the convolution of the inlet concentration and the system response as shown in Equation (21). Solving the convolution integral is a straight forward task, however, the deconvolution problem, that is extracting the response function, $E(t)$, when $C_{out}(t)$ and $C_{in}(t)$ are known, does offer several challenges.

$$C_{out}(t) = \int_0^t C_{in}(t') \cdot E(t-t')\,dt' = \int_0^t C_{in}(t-t') \cdot E(t')\,dt' \qquad (21)$$

Many techniques have been proposed for the solution of the deconvolution problem in chemical engineering applications (Bennia and Nahman, 1990; Boskovic and Loebbecke, 2008; Essadki et al., 2011; Guiterrez et al., 2010; Heibel et al., 2005; Hutter et al., 2011; Häfeli et al., 2013; Mills and Dudukovic, 1989; Moa et al. 1998; Nahman and Guillaume, 1981; Parruck and Riad, 1984; Pasnanakis and Abel, 1998;

Saber et al., 2012; Thakur et al., 2003), where most of them rely on transforming the convolution integral into a multiplication in the frequency of Laplace domains (after applying a Fourier or a Laplace transform), calculating the response function then applying an inverse transform to get the time domain response function (Boskovic and Loebbecke, 2008; Mao et al., 1998). Such approach however is likely to present several hurdles since this transformation amplify the noise from the sensors used for measuring the concentrations, and the use of a proper filtering technique to remove this noise becomes essential. Many studies are dedicated to such filter designs and several filter variants that have been applied with varying degrees of accuracy are available in the literature (Bennia and Nahman, 1990; Hunt, 1971; Mills and Duduković, 1989; Nahman and Guillaume, 1981; Parruck and Riad, 1984). Another technique that is commonly used to solve the deconvolution problem is to assume that the residence time distribution function, *E(t)*, follows a conventional RTD model (e.g. axial dispersion model), which could be a one- or a two-parameter model. The solution of the problem is now reduced to searching for the best model parameters that would minimize the error between the outcome of the convolution integral and the measured outlet concentration (Häfeli et al., 2013).

This latter technique, however, may conceal a large amount of information pertaining to the flow by lumping them into one parameter. Hence, in a fashion similar to the previous work on single phase flow (Abou Hweij and Azizi, 2015) the technique to obtain the distribution function *E(t)* from the inlet and outlet concentration measurements by applying the filter proposed by Mills and Dudukovic (Mills and Dudukovic, 1989) will be employed in the current work. In this approach a second-order smoothing filter is employed to remove the noise from measured data to obtain

the frequency domain impulse response, according to Equation (22) (Mills and Dudukovic, 1989; Abou Hweij and Azizi, 2015).

$$E(\omega) = \frac{C_{out}(\omega)/C_{in}(\omega)}{1+\gamma\dfrac{S(\omega)\cdot S^{*}(\omega)}{C_{in}(\omega)\cdot C_{in}^{*}(\omega)}} \tag{22}$$

Where, γ is the filtering parameter, and the term $\left[\gamma\cdot S(\omega)\cdot S^{*}(\omega)/C_{in}(\omega)\cdot C_{in}^{*}(\omega)\right]$ plays the role of a digital filter. $S(\omega)$ is the FFT of the smoothing formula coefficient series [1, –2, 1, 0, …, 0]; which is a matrix of length *k*, the number of sampling points. The quantities marked with an asterisk (i.e. C_{in}^{*} and S^{*}) denote the complex conjugate of the inlet concentration and the smoothing formula series (Mills and Dudukovic, 1989; Mao et al., 1998; Hunt, 1970, 1971). The length of the matrix, *k*, is equivalent to the number of sampled points in each experimental run.

While the filtering parameter is unbounded and can assume any positive real value ($\gamma \in \mathbb{R}^{+}$), the choice of γ, and the method required to find it is described elsewhere (Mills and Dudukovic, 1989; Abou Hweij and Azizi, 2015).

After calculating $E(\omega)$, the residence time distribution function, *E(t)*, of the reactor can now be obtained by calculating the inverse transform of $E(\omega)$.

$$E(t) = IFFT\left(E(\omega)\right) \tag{23}$$

A user defined function that performs these numerical calculations in Matlab® was used. This in-house code would solve the various equations to obtain the value of the fitting parameter, γ, and consequently the impulse response, *E(t)*. Once the latter function is known, the various moments of the distribution can be calculated (i.e. mean residence time, t_m, and variance, σ^2) further characterization of the reactor can be performed.

$$t_m = \int_0^\infty tE(t)dt \tag{24}$$

$$\sigma^2 = \int_0^\infty (t - t_m)^2 E(t)\,dt = \int_0^\infty t^2 E(t)\,dt - t_m^2 \tag{25}$$

C. Results and Discussion

Various operational parameters as well as reactor/contactor design geometries were varied with the objective of testing their effect on the pressure drop of two phase flow through tubular contactors equipped with screen-type static mixers as well as the liquid-phase residence time distribution in the reactor. The experimental findings of these cases are reported in the following sections.

1. Pressure drop

The only energy cost associated with the operation of a reactor equipped with static mixers is the energy required to pump the flow through it, knowledge of the pressure drop and how it is affected by various operational and design parameters becomes very important for the economics of the process. In the current study, the effect of changing the screen design/geometry (for all screens listed in Table 3) on the pressure drop across the mixing chamber for a turbulently flowing gas-liquid dispersion was investigated under different operating conditions as summarized in Table 4.

Parameter	Operating Conditions
Mixer diameter	37 mm
Number of screens elements	8
Inter-screen spacing, L_{screen}	60 mm
Total length of the mixing section, L_M	600 mm
Distance between pressure transducers, L_p	850 mm
Liquid-phase velocity, U_L	0.25 – 0.75 m/s
Gas-phase velocity, U_G	0.02 – 0.15 m/s
Gas phase holdup, ϕ	0.05, 0.1, and 0.2
Pipe Reynolds number, Re	~ 11,500 –28,000

Table 4 Range of experimental conditions investigated during pressure drop experiments

The effect of introducing a secondary phase, to the turbulent flow of water in the reactor, on the pressure drop in the mixing section is depicted in Figure 23, where the evolution of both the pressure drop and the friction factor, *f*/2, versus the pipe Reynolds number $\left(\mathrm{Re} = D \cdot U_{mix} \cdot \rho / \mu\right)$ is presented. It is very clear that the pressure drop increases with an increase in the dispersed phase volume fraction, ϕ, which is translated into an increase in the friction factor *f*/2, which is defined according to Equation (26). However the friction factor decreases with an increase in the Reynolds number and shows a tendency to plateau at larger Re values.

$$\frac{f}{2} = \frac{\Delta P \cdot D}{4 \cdot L \cdot \rho \cdot U^2} \tag{26}$$

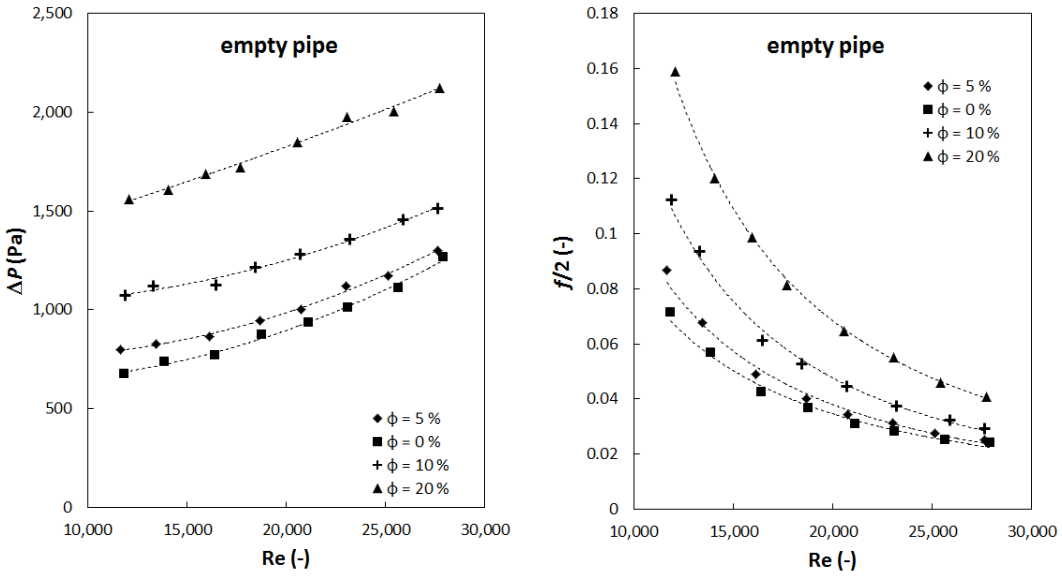

Figure 23: Evolution of the pressure drop and the friction factor, *f*/2, across the mixing chamber for an empty pipe (no screens) as a function of the Reynolds number.

This is in line with the observations of several investigators (Heyouni et al., 2002; Parmar and Majumder, 2014) who reported a decrease in the value of *f* with an increase in Re as well as a tendency for *f* to plateau at system-specific Re values.

Inserting screen-type static mixers in the mixing section presents an additional obstruction to the flow which should be translated into an increase in the pressure drop (or pumping power requirements). This effect is expected to be amplified as the mesh opening of the screen becomes smaller. This is in line with the observations reported in Figure 24 where the change in ΔP vs. Re is presented for the cases of 5% and 20% dispersed phase holdup. In these two cases, the pressure drop clearly increases with an increase in the total flow rate entering the reactor, and/or with a decrease in the mesh opening of the STSM.

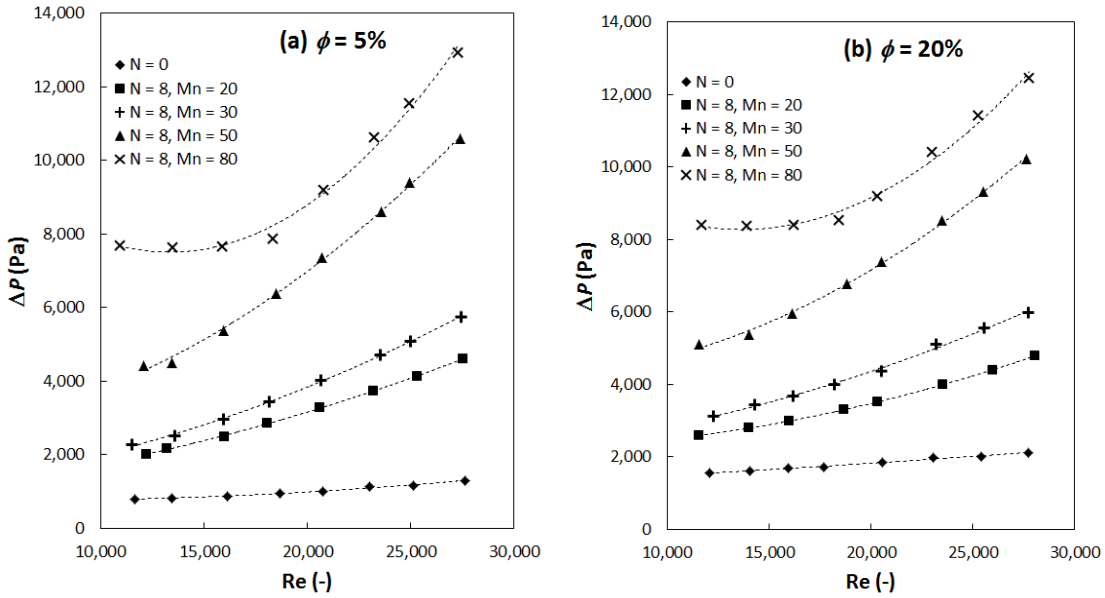

Figure 24: Effect of screen geometry and gas holdup on the pressure drop in the reactor in the presence of 8 screens.

However, an interesting observation pertaining to the effect of introducing a secondary gas phase on the pressure drop in the presence of screen-type static mixers can be noted. On the contrary to the case of an empty pipe, the pressure drop in the presence of screens was found to decrease in the presence of dispersed air with the decrease being more pronounced at larger gas phase volume fractions (cf. Figure 25). This can be attributed to the ability of screens to generate fine bubbles which in turn reduce the drag coefficient, Ψ, of the screens. The screen drag coefficient, Ψ, can be calculated according to Equation (27) using the pressure drop due to screens only. This value, $\Delta P_{screens}$, can be obtained by subtracting the pressure drop in empty pipe from the total measured pressure drop in the presence of screens at the same gas phase holdup, according to Equation (28).

$$\Psi = \frac{\Delta P_{screens}}{(1/2)\rho U^2} \tag{27}$$

$$\Delta P_{screens,i} = \Delta P_{system,i} - \Delta P_{pipe,i} \tag{28}$$

Where subscript *"i"* denotes the holdup of the dispersed phase at which the pressure drop was measured (i.e. for ϕ =5, 10, or 20%).

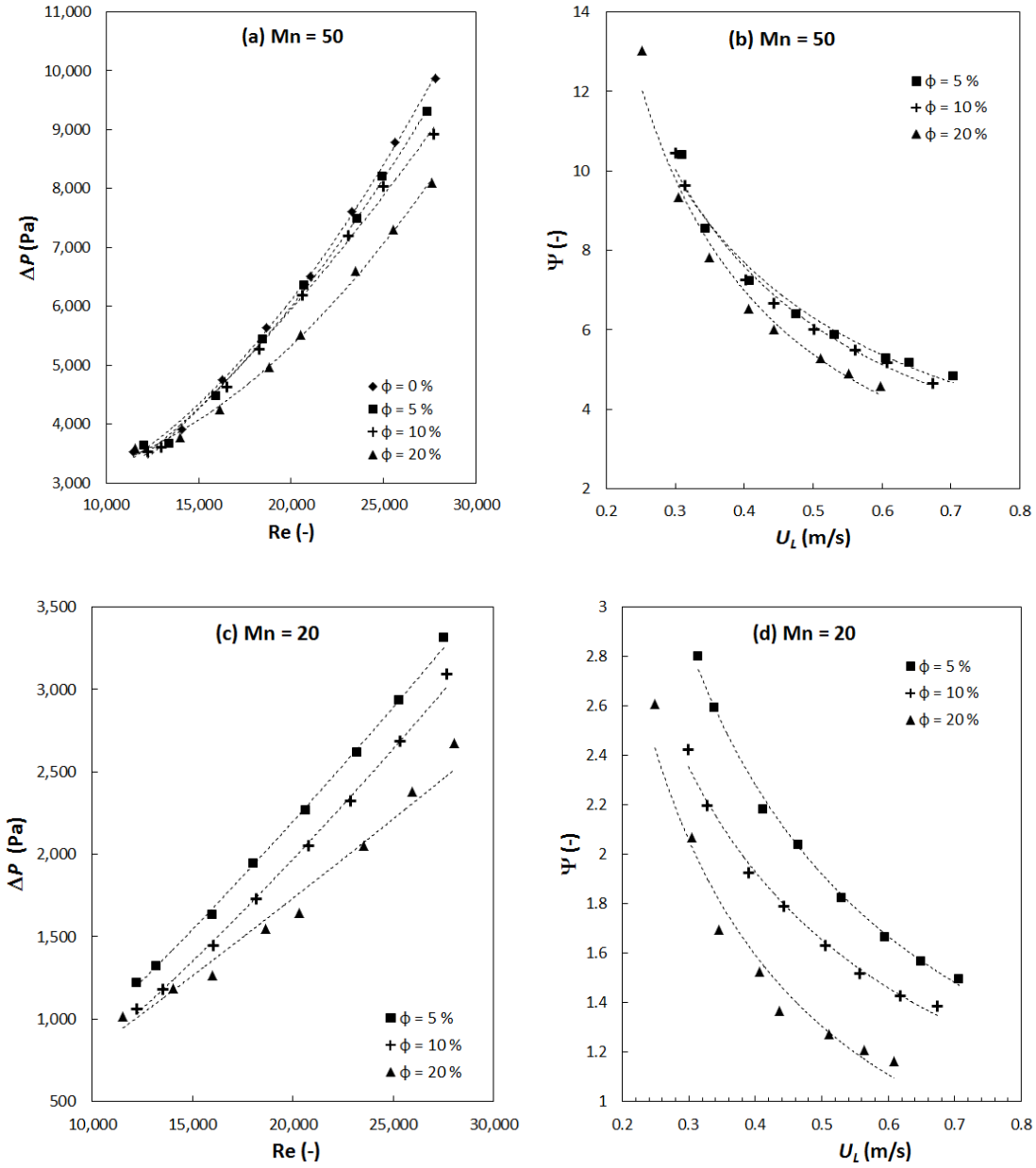

Figure 25: Variation of the pressure drop with Re and the drag coefficient of the screen with the liquid superficial velocity for two different screen geometries.

Unlike the friction factor, f (defined in Equation (26)), the drag coefficient of the screen, Ψ, does not account for the aspect ratio (*thickness or length of one element/diameter of the element*) of the mixing element. This is of great advantage when analyzing flows through screens, because unlike other types of static mixers that

occupy a certain length of the mixing section, screen elements require a small footprint in the pipe with their thickness being equal to twice the wire diameter, *b*.

The drag coefficient of the screen is however a direct function of its geometry. This is clearly presented in Figure 26 which depicts the variation of Ψ with the pipe Reynolds number. Similarly to the empty pipe case, the drag coefficient decreases with an increase in the flow rate entering the reactor. It also increases with a decreasing mesh opening.

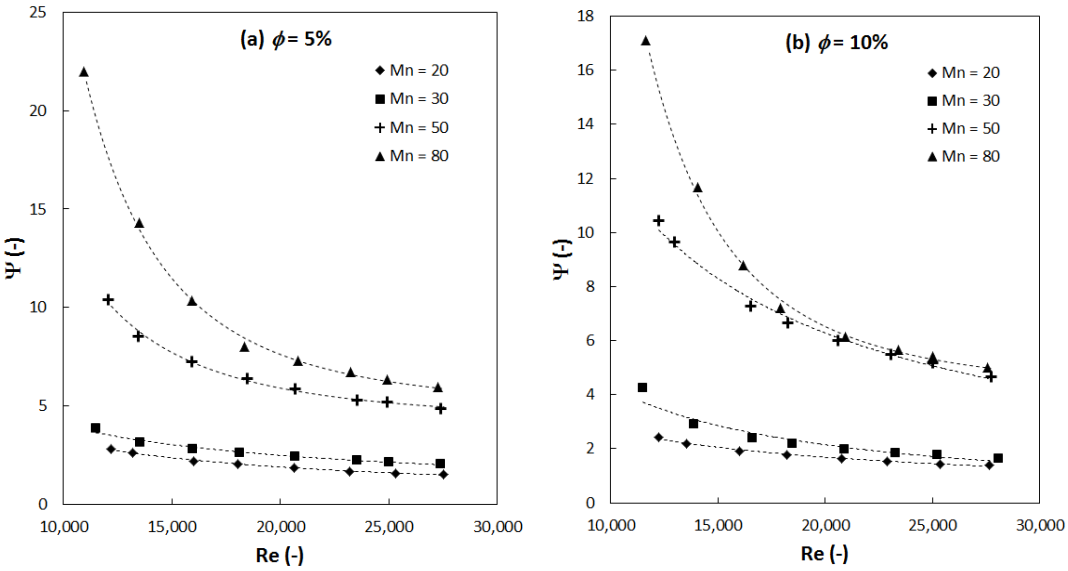

Figure 26: Effect of screen geometry on the value of the screen drag coefficient at various Reynolds numbers for two different gas phase volume fractions.

The drag coefficient data obtained in the current investigation (96 data points) were correlated and good agreement was achieved between the experimental and predicted values, obtained using Equation (29). The parity plot showing this correlation is presented in Figure 27.

$$\Psi = 207.26 \cdot \mathrm{Re}^{-1.03} \cdot \phi^{-0.08} \cdot M^{-0.51} \cdot \alpha^{-2.206} \qquad \left(R^2 = 0.97\right) \qquad (29)$$

Where *M* is in meters (m).

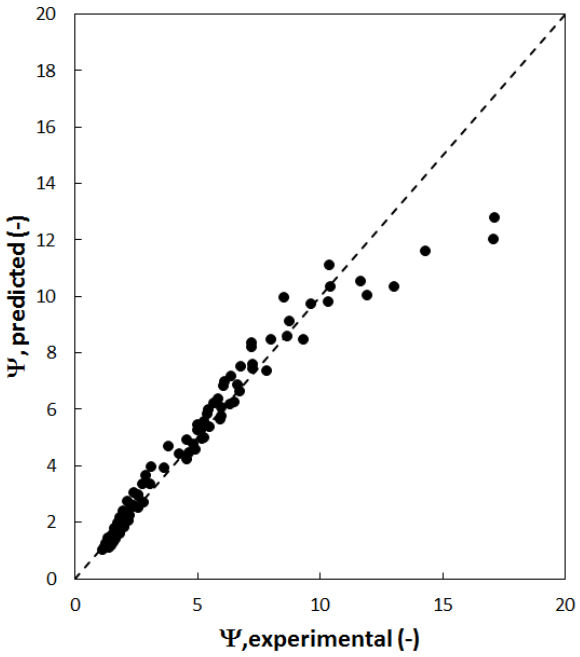

Figure 27: Parity plot for the screen drag coefficient at various operating and design conditions

2. RTD Experiments

Residence time distribution experiments were performed using KCl as the tracer because of the linear relationship between its concentration and conductivity. Similarly to the previous work on single phase flow, the analysis assumed an imperfect pulse technique for which a signal deconvolution was required to obtain the impulse response of the residence time distribution function, *E(t)*. The data was analyzed as presented in the work of Abou Hweij and Azizi (2015) where the raw conductivity measurements were conditioned to remove the background conductivity of RO water and then transformed in concentration measurements which in turn were normalized according to Equation (30).

$$C(t) = \frac{C_{raw}(t)}{\int_0^\infty C_{raw}(t)\,dt} \tag{30}$$

All experimental runs were conducted a minimum of four times to ensure repeatability of the results, especially that the conductivity sensors showed some noise in the signal due to the introduction of a secondary phase of negligible conductivity. In addition, a mass balance was conducted on each of these runs to check if the two sensors are measuring a comparable amount of salt (mass conservation) in the system and it was found that the difference between the inlet and outlet recorded amounts of KCl varied by 19.7% on average.

Using an in-house computational subroutine that would perform the deconvolution using the method presented by Mills and Dudukovic (1989), *E(t)* was obtained for each experimental run. While solving the deconvolution problem, the subroutine ensures that the first and second moments of the RTD function are conserved. Further information about its accuracy and the additional time-domain smoothing required to obtain *E(t)* are described elsewhere (Abou Hweij and Azizi, 2015).

To check the accuracy of the approach and validate the data, the convolution integral described in Equation (21) was performed on most calculated results to check if the convolution of the normalized inlet concentration with the calculated *E(t)* would match the normalized outlet concentration. Figure 28(a) and (b) show the results of this convolution and a good match was always obtained, which indicates that the computed RTD renders an accurate description of the macromixing behavior of the system.

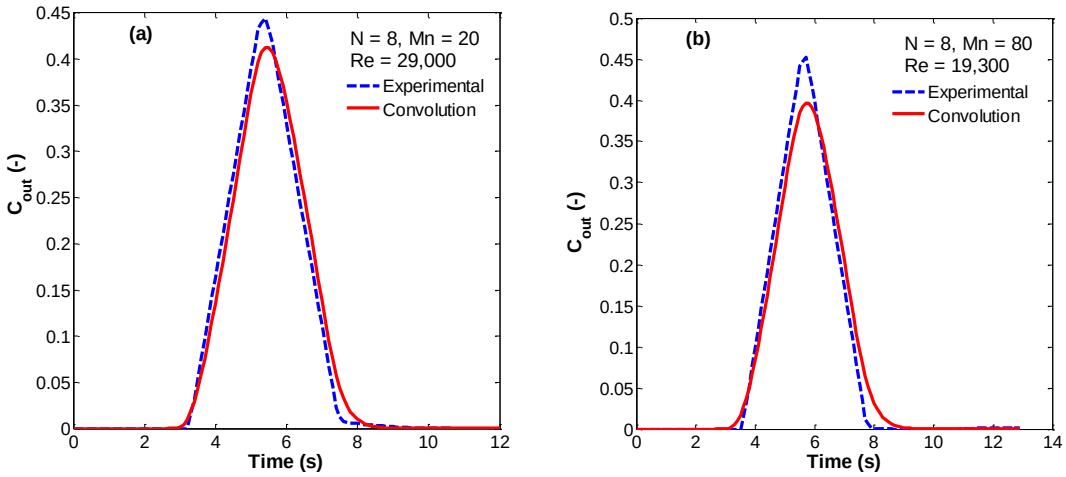

Figure 28: Normalized outlet concentration, experimental vs. convolution of inlet concentration and calculated impulse response.

a. Effect of flow velocity on RTD

A higher flow velocity dictates a shorter residence time in the mixing section and therefore the RTD function, E(t) is expected to become narrower and shifted towards shorter times. This is clearly observed in Figure 29(a) and (c) where the narrower E(t) is clearly observed at higher Re for two different screen geometries. However, a proper interpretation and comparison between the various RTD functions can only be performed after using the dimensionless time , Θ, which is defined as the ratio of the time, t, to the mean residence time, t_m, $\left(\Theta = t/t_m\right)$. Under these conditions, it becomes very clear that the dimensionless distribution E(Θ), broadens with an increase in the flow rate entering the mixing section (cf. Figure 29(b) and (d)). This is an indication of the increase in the axial dispersion coefficient with an increase in the flow velocity.

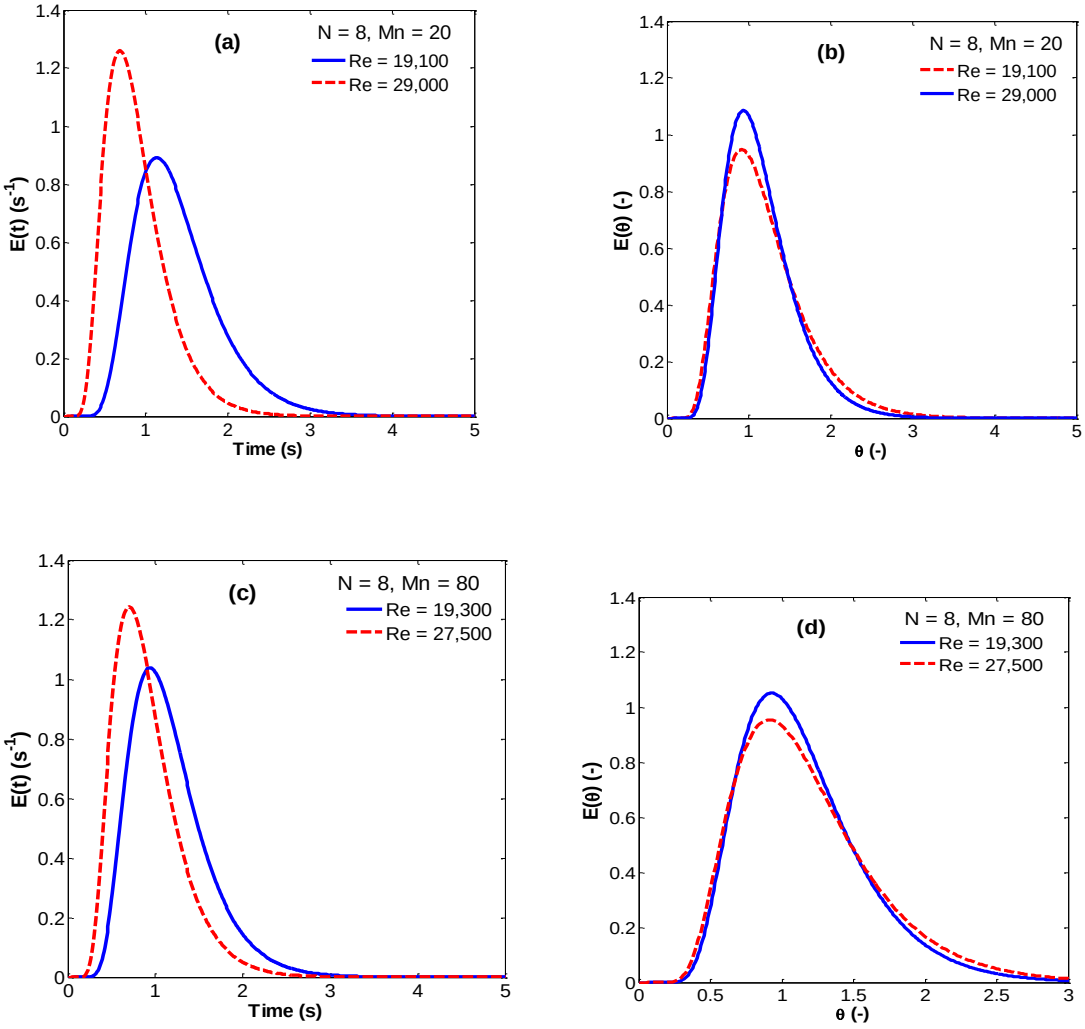

Figure 29: Effect of flow velocity on $E(t)$ and $E(\theta)$ for various operating conditions and screen geometries.

Using the well-known one parameter model, presented in Equation (31), that describes the evolution of the axial dispersion as a function of time, the Péclet number, Pe, can be approximated by fitting Equation (31) to the experimental determined E(t) function.

$$E(\Theta) = t_m \cdot E(t) = \frac{1}{2} \cdot \sqrt{\frac{Pe}{\pi \cdot \Theta}} \cdot \exp\left(-\frac{Pe \cdot (1-\Theta)^2}{4 \cdot \Theta} \right) \qquad (31)$$

The value of Pe is then used to compute the axial dispersion coefficient, D_{ax}. The Péclet number for a tube flow is defined as $Pe = L \cdot U / D_{ax}$, where L is the mixing chamber length, and U is the mean flow velocity.

The value of the axial dispersion coefficient, D_{ax}, and how it is affected by the flow velocity is presented in Figure 30(a) and (b) for two different screen geometries. From these figures, it can be clearly noted that the axial dispersion coefficient increases with an increase in the mixture velocity; in addition, inserting a larger number of STSM in the reactor increases the value of D_{ax}. However, the measured D_{ax} remains slightly smaller than that for a two-phase flow in an empty pipe. This highlights the fact that the presence of STSM helps better homogenizing the flow in tubular reactors/contactors.

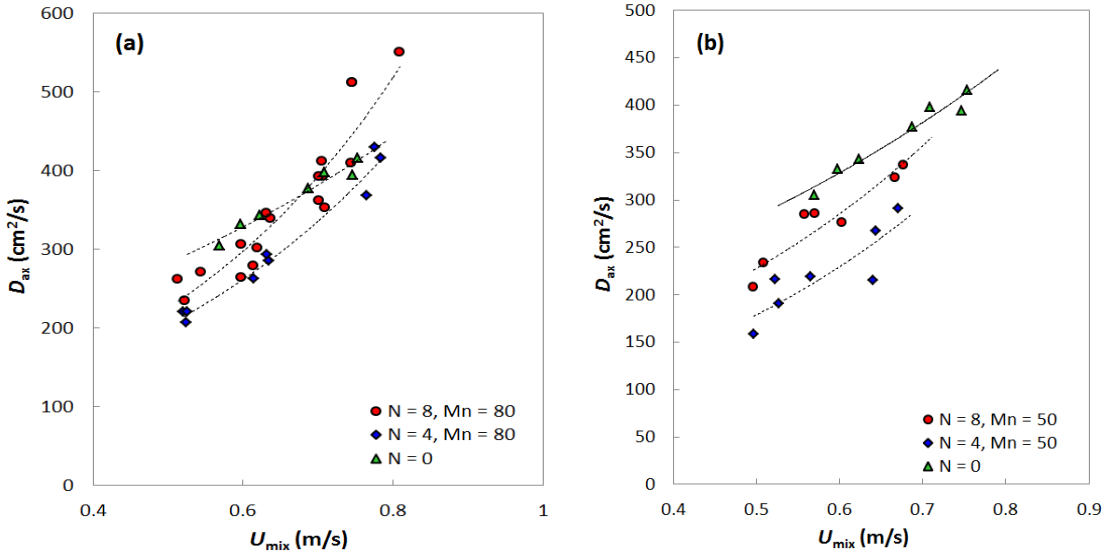

Figure 30: Variation of the liquid-phase axial dispersion coefficient with the average mixture velocity for different screen geometries and number of screen elements (a) Mn = 80, (b) Mn = 50.

b. Effect of screen geometry

To investigate the effect of varying the screen geometry on the liquid-phase axial dispersion in a turbulently flowing gas-liquid dispersion through STSM, the axial dispersion coefficient was plotted against the pipe Reynolds number in Figure 31a for the various screen geometries presented in Table 3. It is very clear that the calculated

D_{ax} fall in a very narrow region next to each other and no significant conclusion can be drawn from such a figure. However, the calculation of the Reynolds number relies on the definition of the velocity and/or the characteristic length against which it is computed. In the case at hand, four distinct Re variants can be found or calculated, the definition of which is presented in Table 5. Plotting the data against any of these variants was found to render a different conclusion pertaining to the variation of D_{ax} in the mixing section.

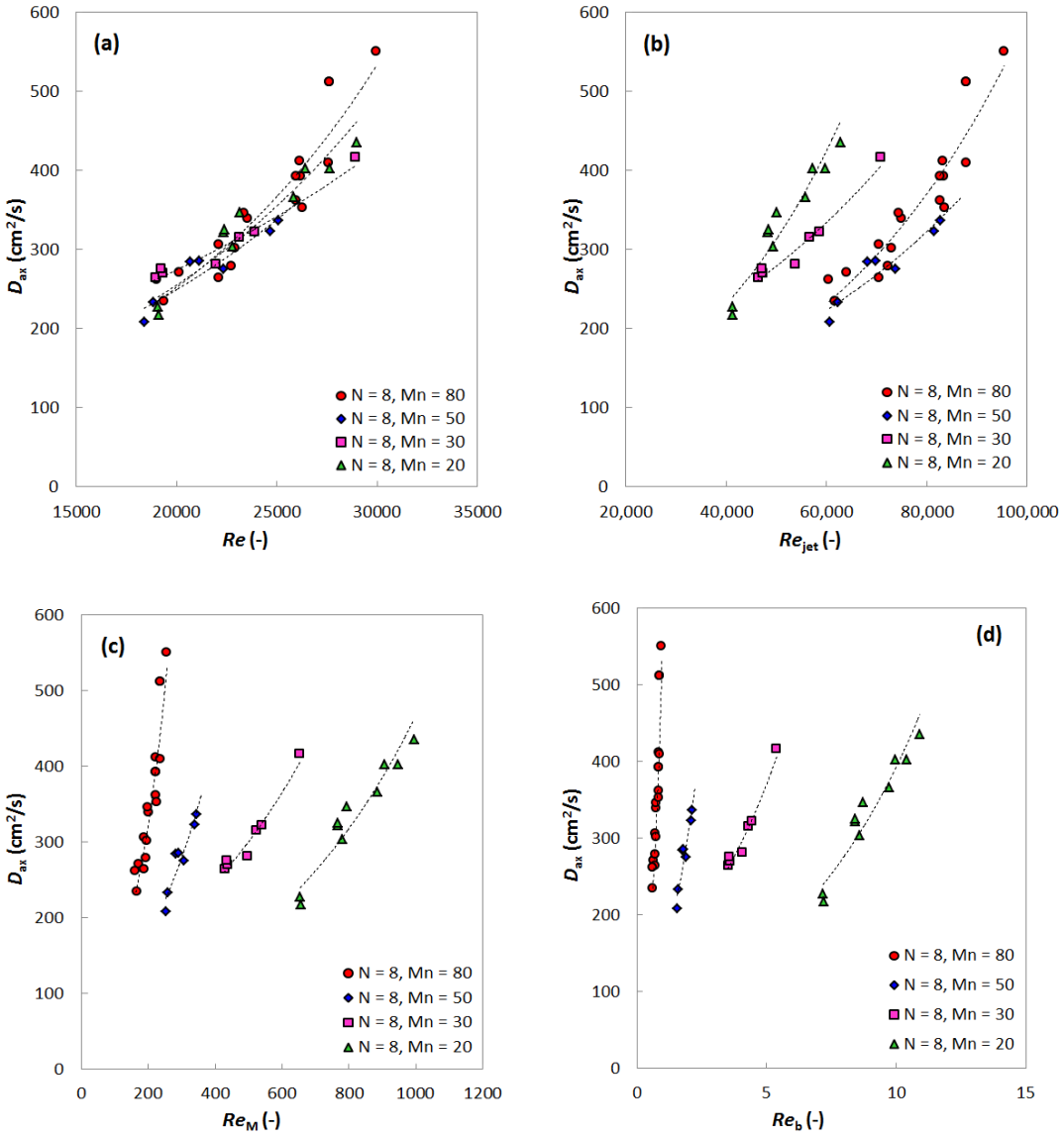

Figure 31: Effect of the Reynolds number characteristic length on the axial dispersion coefficient.

Figure 31b shows the variation of the axial dispersion coefficient with the macroscopic jet Reynolds number. Because Re_{jet} is a direct function of the screen open area, α, and while it is clear that D_{ax} increases with an increase in Re_{jet}, the data showed that the extent of increase in the value of axial dispersion decreases when the screen open area becomes smaller (cf. Table 3). This however is overturned when the characteristic length of the Reynolds number is changed to the mesh opening or the wire diameter of the STSM. While both *M* and *b* decrease with an increasing mesh number, the data show that the axial dispersion is amplified when using smaller mesh openings and wire diameters, i.e. with an increasing mesh number.

Reynolds number	**Value**
Pipe Reynolds number, Re	$D \cdot U_{mix} \cdot \rho / \mu$
Macroscopic jet Reynolds number, Re_{jet}	$D \cdot (U_{mix} / \alpha) \cdot \rho / \mu$
Mesh Reynolds number, Re_M	$M \cdot U_{mix} \cdot \rho / \mu$
Wire Reynolds number, Re_b	$b \cdot U_{mix} \cdot \rho / \mu$

Table 5 Various definitions of the Reynolds number

The choice of the Reynolds number definition and its characteristic length is therefore of paramount importance when trying to design tubular reactors/contactors equipped with STSM as it will dictate the extent of axial dispersion. Furthermore, these findings are in line with the observations reported for single phase flow through STSM (Abou Hweij and Azizi, 2015) where the importance of defining the appropriate Re has been highlighted.

c. Comparison with flow in an empty pipe and regression analysis

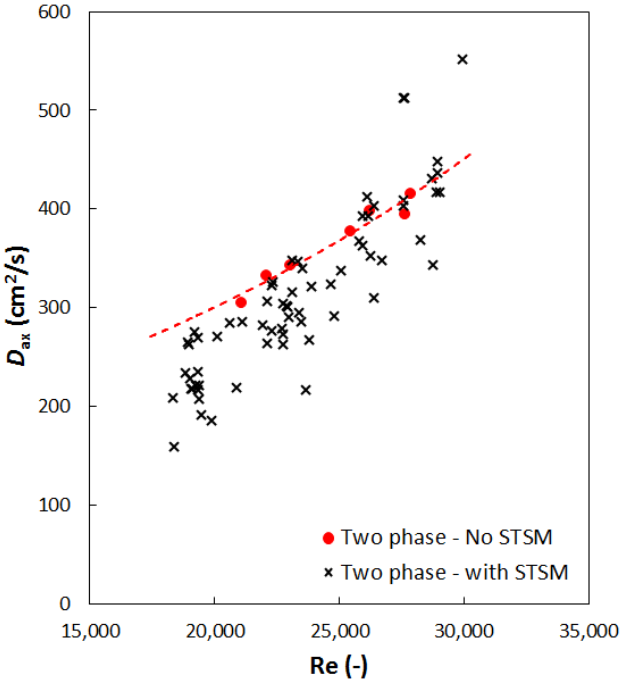

Figure 32: Comparison between the axial dispersion in the presence of screens with that for an empty pipe when plotted against the empty pipe Reynolds number, Re.

The advantages of utilizing screen-type static mixers are highlighted in Figure 32, which shows the calculated liquid-phase axial dispersion coefficient, D_{ax}, for all experimental runs plotted against those for the runs where no static mixers were inserted in the pipe. When all the parameters are lumped together (i.e. number of screen elements, screen geometry, and flow velocity) it is very evident that screen-type static mixers allow for a smaller axial dispersion when compared to an empty pipe and therefore a better mixing performance.

The data obtained in the current work were then correlated in order to be able to predict the performance of the mixer.

$$D_{ax}\left(cm^2/s\right) = 0.003\cdot \mathrm{Re}^{2.481}\cdot\left(M-b\right)^{-1.015}\cdot N^{0.233}\cdot\phi^{0.004}\cdot \mathrm{Re}_b^{0.427}\cdot \mathrm{Re}_{jet}^{-1.374} \quad \left(R^2 = 0.903\right) \tag{32}$$

Where M and b are in mm.

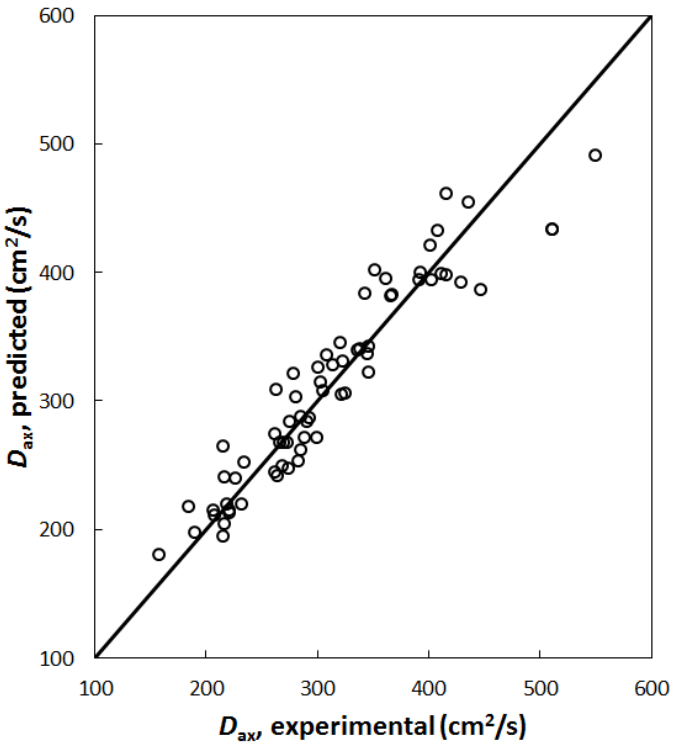

Figure 33: Parity plot for the predicted vs. experimental axial dispersion coefficient values

It is very clear from Equation (32), and on the contrary to the case of single phase flow (Abou Hweij and Azizi, 2015), the effect of the number of screen elements is of considerable significance in the case of two phase gas-liquid flow. However, the effect of dispersed phase holdup appears to have a minor role.

D. Conclusions

This study investigated the hydrodynamics and residence time distribution of two-phase gas-liquid flow in tubular reactors equipped with screen-type static mixers. While the pressure drop was found to be a direct function of the mesh opening of every STSM, the ability of these mixers to generate fine bubbles was found to be beneficial in terms of reducing the drag coefficient of the screen and hence lowering the pumping

requirement to drive the flow in the presence of a secondary gaseous phase, the extent of which increases with an increase in the dispersed phase volume fraction.

Furthermore, the axial dispersion coefficient was found to increase with an increase in the total flow rate entering the mixing section while being a direct function of the number of inserted mixing elements and the screen geometry. The latter effect (i.e. screen geometry) however is directly related to the definition of the Reynolds number against which we are comparing the results. Deciding which characteristic length to use is therefore the responsibility of the user of these STSM and would be related to the operation being undertaken. However, the axial dispersion coefficient was found to be lower in most cases than that measured in gas-liquid pipe flows operating under the same conditions but without the insertion of static mixers.

CHAPTER III

GENERAL CONCULSIONS

- This study investigated the hydrodynamics and residence time distribution liquid single phase and two-phase gas-liquid flow in tubular reactors equipped with screen-type static mixers.
- Pressure drop through various screen geometries and under different operating conditions was found to be a direct function of their mesh opening and screen fraction open area in both studies.
- In both single phase liquid and two-phase gas-liquid flow, the axial dispersion coefficient in reactors equipped with screen mixers increases with an increasing flow velocity and this data could be interpreted in terms of various Reynolds numbers, depending on the characteristic length used.
- Axial dispersion was found not to be affected by the number of screen elements in the pipe significantly in single phase liquid flow while showing a direct function with the number of screens inserted in the two phase flow.
- Screen-type static mixers allow for a smaller axial dispersion when compared to an empty pipe and therefore a better mixing performance in both single phase and two-phase gas-liquid flow.

BIBLIOGRAPHY

A. Bennani, J. N. Gence, J. Mathieu, The influence of a grid-generated turbulence on the development of chemical reactions, AIChE journal 31.7 (1985): 1157-1166.

A. Bennia, N.S. Nahman, Deconvolution of System Impulse Responses and Time Domain Waveforms, IEEE Trans. Instrum. Meas. 79 (1990) 933–939.

A. Ghanem, T. Lemenand, D. Della Valle, H. Peerhossaini, Static mixers: Mechanisms, applications, and characterization methods–A review, Chem. Eng. Res. Des. 92 (2014) 205–228.

A. Heyouni, M. Roustan, Z. Do-quang, Hydrodynamics and Mass Transfer in Gas – Liquid through Static Mixers, Chemical Engineering Science, (2002), 57, 3325–3333.

A. M. Al Taweel, C. Chen, A novel static mixer for the effective dispersion of immiscible liquids, Chemical engineering research & design 74.4 (1996): 445-450.

A. Peschel, B. Hentschel, H. Freund, K. Sundmacher, Design of optimal multiphase reactors exemplified on the hydroformylation of long chain alkenes, Chem. Eng. J. 188 (2012) 126–141.

A.H. Essadki, B. Gourich, C. Vial, H. Delmas, Residence time distribution measurements in an external-loop airlift reactor: Study of the hydrodynamics of the liquid circulation induced by the hydrogen bubbles, Chem. Eng. Sci. 66 (2011) 3125–3132. doi:10.1016/j.ces.2011.02.063.

A.K. Heibel, P.J.M. Lebens, J.W. Middelhoff, F. Kapteijn, J. Moulijn, Liquid residence time distribution in the film flow monolith reactor, AIChE J. 51 (2005) 122–133. doi:10.1002/aic.10288.

A.M. Al Taweel, C. Li, H.G. Gomaa, P. Yuet, Intensifying mass transfer between immiscible liquids: Using screen-type static mixers, Chem. Eng. Res. Des. 85 (2007) 760–765. http://dx.doi.org/10.1205/cherd06180;

A.M. Al Taweel, F. Azizi, G. Sirijeerachai, Static mixers: Effective means for intensifying mass transfer limited reactions, Chem. Eng. Process. Process Intensif. 72 (2013) 51–62. doi:10.1016/j.cep.2013.08.009.

A.M. Al Taweel, J. Yan, F. Azizi, D. Odedra, H.G.G. Gomaa, Using in-line static mixers to intensify gas–liquid mass transfer processes, Chem. Eng. Sci. 60 (2005) 6378–6390. doi:10.1016/j.ces.2005.03.011.

B. Parruck, S.M. Riad, Study and Performance Evaluation of Two Iterative Frequency-Domain Deconvolution Techniques, IEEE Trans. Instrum. Meas. 33 (1984) 281–287.

B.R. Hunt, Biased estimation for nonparametric identification of linear systems, Math. Biosci. 10 (1971) 215–237. doi:10.1016/0025-5564(71)90061-7.

B.R. Hunt, The inverse problem of radiography, Math. Biosci. 8 (1970) 161–179. doi:10.1016/0025-5564(70)90148-3.

C. Chen, Dispersion and coalescence in static mixers, Technical University of Nova Scotia, 1996.

C. Hutter, a. Zenklusen, R. Lang, P. Rudolf von Rohr, Axial dispersion in metal foams and streamwise-periodic porous media, Chem. Eng. Sci. 66 (2011) 1132–1141. doi:10.1016/j.ces.2010.12.016.

C. M. R. Madhuranthakam, Q. Pan, G. L. Rempel, Residence time distribution and liquid holdup in Kenics KMX static mixer with hydrogenated nitrile butadiene rubber solution and hydrogen gas system, Chemical Engineering Science, 64(14), (2009): 3320-3328.

C.G.C.C. Gutierrez, E.F.T.S. Dias, J. a. W. Gut, Residence time distribution in holding tubes using generalized convection model and numerical convolution for non-ideal tracer detection, J. Food Eng. 98 (2010) 248–256. doi:10.1016/j.jfoodeng.2010.01.004.

C.K. Harris, D. Roekaerts, F.J.J. Rosendal, F.G.J. Buitendijk, P. Daskopoulos, A.J.N. Vreenegoor, et al., Computational fluid dynamics for chemical reactor engineering, Chem. Eng. Sci. 51 (1996) 1569–1594. http://dx.doi.org/10.1016/0009-2509(96)00021-8.

C.M.R. Madhuranthakam, Q. Pan, G.L. Rempel, Hydrodynamics in Sulzer SMX Static Mixer with Air/Water System, Ind. Eng. Chem. Res. 48 (2009) 719–726. http://pubs.acs.org/doi/abs/10.1021/ie801407y.

D. Boskovic, S. Loebbecke, Modelling of the residence time distribution in micromixers, Chem. Eng. J. 135 (2008) S138–S146. doi:10.1016/j.cej.2007.07.058.

D. Pananakis, E.W. Abel, A comparison of methods for the deconvolution of isothermal DSC data, Thermochim. Acta. 315 (1998) 107–119.

D. Ziolkowski, J. Morawski, The flow characteristic of the liquid streams inside a tubular apparatus equipped with static mixing elements of a new type, Chem. Eng. Process. 21 (1987) 131–139.

E. Lobry, F. Theron, C. Gourdon, N. Le Sauze, C. Xuereb, T. Lasuye, Turbulent liquid–liquid dispersion in SMV static mixer at high dispersed phase concentration, Chemical Engineering Science, 66(23), (2011):5762-5774.

E.B. Nauman, D. Kothari, K.D.P. Nigam, Static Mixers to Promote Axial Mixing, Chem. Eng. Res. Des. 80 (2002) 681–685. doi:10.1205/026387602760312890.

E.B. Nauman, Reactions and residence time distributions in motionless mixers, Can. J. Chem. Eng. 60 (1982) 136–140. doi:10.1002/cjce.5450600123.

E.B. Nauman, Residence Time Theory, Ind. Eng. Chem. Res. 47 (2008) 3752–3766.

F. Azizi, A. M. Al Taweel, Population balance simulation of gas–liquid contacting, Chemical Engineering Science 62.24 (2007): 7436-7445.
F. Azizi, A. M. Al Taweel, Hydrodynamics of liquid flow through screens and screen-type static mixers, Chemical Engineering Communications 198.5 (2011): 726-742.

F. Azizi, A.M. Al Taweel, Inter-phase mass transfer in turbulent liquid-liquid dispersions: A comparative analysis of models, Chem. Eng. J. 179 (2012) 231–241. doi:10.1016/j.cej.2011.10.063.

F. Azizi, A.M. Al Taweel, Turbulently flowing liquid–liquid dispersions. Part I: Drop breakage and coalescence, Chem. Eng. J. 166 (2011) 715–725. doi:10.1016/j.cej.2010.11.050.

F. Azizi, Design and Operation of Intensified Multiphase Processes, (2009).

F. Theron, N. Le Sauze, A. Ricard, Turbulent Liquid - Liquid Dispersion in Sulzer SMX Mixer, Ind. Eng. Chem. Res. 49 (2010) 623–632.

F. Theron, N. Le Sauze, Comparison between three static mixers for emulsification in turbulent flow, Int. J. Multiph. Flow. 37 (2011) 488–500. doi:10.1016/j.ijmultiphaseflow.2011.01.004.

F. Theron, N. Le Sauze, Comparison between three static mixers for emulsification in turbulent flow, Int. J. Multiph. Flow. 37 (2011) 488–500. doi:10.1016/j.ijmultiphaseflow.2011.01.004.

G. U. Din, I. R. Chughtai, M. H. Inayat, I. H. Khan, Axial dispersion, holdup and slip velocity of dispersed phase in a pulsed sieve plate extraction column by radiotracer residence time distribution analysis, Applied Radiation and Isotopes, *66*(12), (2008): 1818-1824.

H.S. Fogler, Elements of chemical reaction engineering, (1999).

H.Z. Li, C. Fasol, L. Choplin, Pressure drop of Newtonian and non-Newtonian fluids across a Sulzer SMX static mixer, Chem. Eng. Res. Des. 75 (1997) 792–796.

I. Langmuir, The velocity of reactions in gases moving through heated vessels and the effect of convection and diffusion. J. Am. Chem. Soc., 30, 1742 (1908)
J. R. Bourne, M. Lips, Micromixing in grid- generated turbulence: theoretical analysis and experimental study, The Chemical Engineering Journal 47.3 (1991): 155-162.

J.R. Bourne, M. Lips, Micromixing in grid-generated turbulence. Theoretical analysis and experimental study, Chem. Eng. J. Biochem. Eng. J. 47 (1991) 155–162. http://dx.doi.org/10.1016/0300-9467(91)85021-M.

K. Abou Hweij, F. Azizi, Hydrodynamics and Residence Time Distribution of Liquid Flow in Tubular Reactors Equipped with Screen-type Static Mixers, *under review*, Chemical Engineering Journal (2015).

M. Rafiee, M.J.H. Simmons, A. Ingram, E.H. Stitt, Development of Positron Emission Particle Tracking for Studying Laminar Mixing in Kenics Static Mixer, in: 14th Eur. Conf. Mix., Warszawa, Poland, 2013: pp. 389–394.

M. Saber, C. Pham-Huu, D. Edouard, Axial Dispersion Based on the Residence Time Distribution Curves in a Millireactor Filled with β-SiC Foam Catalyst, Ind. Eng. Chem. Res. 51 (2012) 15011–15017. doi:10.1021/ie3017829.

N.S. Nahman, M.E. Guillaume, Deconvolutlon of Time Domain Waveforms in the Presence of Noise, Boulder, CO, 1981.

O. Levenspiel, Chemical reaction engineering, Wiley New York etc., 1972.

P. Pustelnik, Investigation of Residence Time Distribution in Kenics Static Mixers, Chem. Eng. Process. 20 (1986) 147–154.

P. V. Danckwerts, Continuous-flow systems, Distribution of residence times, Chem. Eng. Sci., 2, (1953)

P.L. Mills, M.P. Duduković, Convolution and Deconvolution of Nonideal Tracer Response Data with Application Three-Phase Packed-Beds, Comput. Chem. Eng. 13 (1989) 881–898.

P.V. Danckwerts, Continuous flow systems, Distribution of Residence Times, Chem. Eng. Sci. 2 (1953) 1–13. doi:10.1016/0009-2509(53)80001-1.

R. Häfeli, C. Hutter, M. Damsohn, H. Prasser, P. Rudolf, V. Rohr, Dispersion in fully developed flow through regular porous structures : Experiments with wire-mesh sensors, Chem. Eng. Process. Process Intensif. 69 (2013) 104–111.

R. Parmar, S. K. Majumder, Hydrodynamics of Microbubble Suspension Flow in Pipes. Industrial and Engineering Chemistry Research, (2014), 53, 3689–3701.

R. Wadley, M.K. Dawson, LIF measurements of blending in static mixers in the turbulent and transitional flow regimes, Chem. Eng. Sci. 60 (2005) 2469–2478. doi:10.1016/j.ces.2004.11.021.

R.K. Thakur, C. Vial, K.D.P. Nigam, E.B. Nauman, G. Djelveh, Static mixers in the process industries - a review, Chem. Eng. Res. Des. 81 (2003) 787–826. http://dx.doi.org/10.1205/026387603322302968.

T.R. Keshav, P. Somaraju, K. Kalyan, A.K. Saroha, K.D.P. Nigam, Liquid phase residence time distribution for gas-liquid flow in Kenics static mixer, Chem. Eng. Process. Process Intensif. 47 (2008) 2275–2280.

V. Kumar, V. Shirke, K.D.P. Nigam, Performance of Kenics static mixer over a wide range of Reynolds number, Chem. Eng. J. 139 (2008) 284–295. doi:10.1016/j.cej.2007.07.101.

Z. Kemblowski, P. Pustelnik, Residence time distribution of a power-law fluid in Kenics static mixers, Chem. Eng. Sci. 43 (1988) 473–478.

Z.-S. Mao, T. Xiong, J. Chen, Residence Time Distribution of Liquid Flow in a Trickle Bed Evaluated Using Fft Deconvolution, Chem. Eng. Commun. 169 (1998) 223–244. doi:10.1080/00986449808912730.

APPENDIX

The pressure drop data was found to better correlate using another regression line of a different form which employs various Reynolds numbers that are based on different characteristic lengths. This regression line is presented in Equation (33), and its corresponding parity plot is shown in Figure 34.

$$\sqrt{\Delta P} = 34.91\alpha - 4909.7b + 7.6\times10^{-3}\,\mathrm{Re}_{jet} - 0.399\,\mathrm{Re}_b + 0.095\,\mathrm{Re}_M \qquad \left(R^2 = 0.999\right) \tag{33}$$

Where ΔP is in Pa, b in m, and Re_b is the wire Reynolds number, $\mathrm{Re}_b = b \cdot U \cdot \rho / \mu$

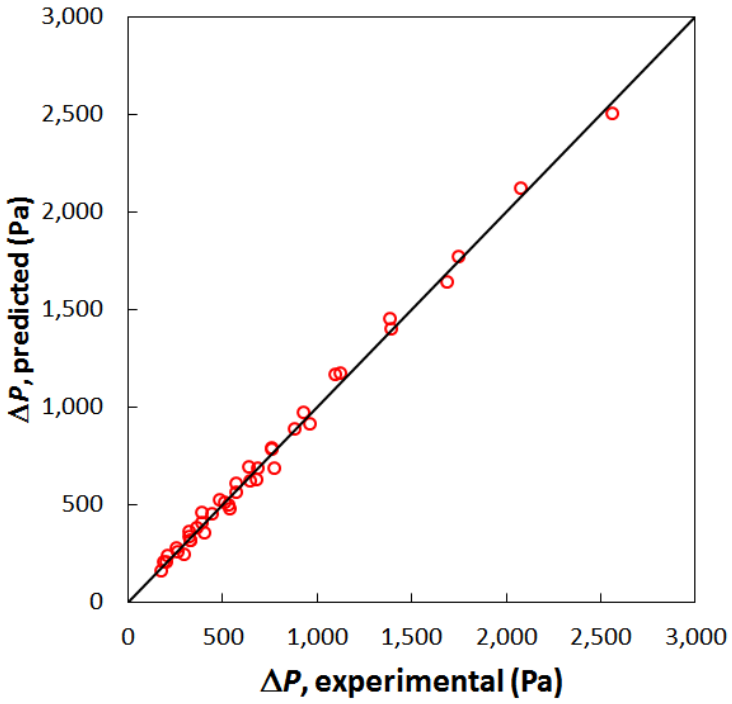

Figure 34: Parity plot for the pressure drop using various Reynolds numbers